THE ASTROPHYSICAL JOURNAL, 259:282–301, 1982 August 1

THE THEORY OF RADIATIVELY DRIVEN STELLAR WINDS. II. THE LINE ACCELERATION

DAVID C. ABBOTT
Joint Institute for Laboratory Astrophysics, University of Colorado and National Bureau of Standards
Received 1981 December 10; accepted 1982 February 19

ABSTRACT

Numerical values of the radiation pressure on spectral lines are presented for the envelopes of stars with spectral type O–G, and with any luminosity, metallicity, or velocity structure. The line acceleration was calculated using a tabulation of atomic lines that is complete for the elements H–Zn. The line acceleration is remarkably constant over the temperature range $50{,}000 \geq T_{\rm eff} \geq 10{,}000$ K, but drops off sharply for cooler stars. The anomalous ionization observed in OB stars decreases the acceleration by up to a factor of 2 from radiative equilibrium values. More than one-half of the acceleration comes from lines whose frequencies overlap with those of neighboring lines at some point in the wind. Line blanketing of the continuum flux by the wind becomes significant for mass loss rates exceeding $\sim 10^{-6}\ M_\odot\ {\rm yr}^{-1}$.

The predicted and observed mass loss rates are in complete agreement for the OB stars, and we conclude that radiation pressure is the dominant mechanism driving the winds from these stars. The mass loss rates of Wolf-Rayet stars are not explained by these models, even accounting for the effects of chemical enrichment on the line acceleration. Radiation-driven mass loss is still significant in F and G supergiants, but the predicted rates are smaller than for OBA supergiants of comparable luminosity. The predicted mass loss rate scales nearly linearly with metallicity, with obvious consequences for stellar systems formed in regions of very high, or very low, metallicity.

Subject headings: stars: early-type — stars: mass loss — stars: supergiants — stars: winds — stars: Wolf-Rayet

I. INTRODUCTION

Stellar winds are observed in O-type stars, A and B supergiants, Wolf-Rayet stars, and the central stars of planetary nebulae (e.g., Conti 1978). These stars are all hot and highly luminous for their mass, which led to the development of a radiation-driven wind theory to explain the mass loss (e.g., Cassinelli 1979). In this model, momentum is transferred from the radiation field to the gas by scattering of radiation in spectral lines. The realism of these models is therefore limited primarily by the accuracy of the calculated line acceleration.

The first modern-day calculation of the radiation force was by Lucy and Solomon (1970), who demonstrated that line scattering in OB stars is so efficient that the radiative momentum absorbed by a single, strong line can overcome gravity. Castor, Abbott, and Klein (1975, hereafter CAK) showed that the acceleration by many weaker lines is a factor of 100 greater than that from the few, strong resonance lines considered by Lucy and Solomon. CAK estimated the line acceleration from all heavy elements using a complete line list for the C III ion. More elaborate calculations by Castor, Abbott, and Klein (1976), as well as Lamers and Morton (1976), confirmed that the line acceleration results from the contribution from a large number of lines and many different elements, many with wavelengths in the Lyman continuum where they cannot be observed.

It has yet to be shown by a quantitative calculation, however, that there are sufficient lines to drive the mass loss observed from these stars. In addition, the dependence of the line acceleration on temperature, density, and chemical composition is needed to compare theory to the wide variety of stars now observed to have winds. This is the motivation for the present paper, which gives improved numerical calculations of the line acceleration in expanding atmospheres of hot stars. Values of the acceleration are tabulated for a sufficiently broad range of effective temperatures, densities, and elemental abundances so that stellar wind models can be generated from this data using the hydrodynamic equations discussed in Paper I (Abbott 1980). Examples of such wind models will be given in Paper III of this series.

To properly calculate the line acceleration, one must solve the radiative transfer problem and tabulate the line opacity. The major improvement of these calculations over previous work is the line opacity, which was computed using a list of atomic lines and *gf*-values that is essentially complete for the first to sixth stages of ionization of the elements H–Zn. Section II describes the atomic data and the method used to calculate the acceleration.

The resulting line acceleration is given in § III. The acceleration is remarkably insensitive to temperature, depends weakly on density, and increases with metallicity. We also estimate bounds on the uncertainty in the acceleration because of the effects of overlapping lines and the effects of anomalous ionization in the wind.

The line acceleration is not directly observable. To compare theory and observation, the equation of motion must be solved using these accelerations and a model for the wind. Section IV uses the CAK wind model to address the questions: (1) Are there sufficient lines to drive the observed mass loss? (2) What spectral regions suffer the most severe line blocking? (3) How do the mass loss rate and the terminal velocity scale with stellar luminosity, effective temperature, mass, and radius? (4) Does the dependence of the radiation force on chemical composition account for the large mass loss rates of the Wolf-Rayet stars and their observed distribution with galactic radius?

II. METHOD

a) *Atomic Data*

i) *Selection of Lines*

The first step in compiling atomic data is to identify which lines from which elements are potential contributors to the acceleration. CAK showed that, once a line becomes optically thick, the amount of momentum absorbed depends only on the value of the velocity and the radiation flux, and not on the line opacity. Stronger lines contribute no more than weaker lines, so long as both are optically thick. As a first criterion, a realistic calculation of the acceleration should therefore include all lines which could potentially be optically thick under conditions expected in the winds of hot stars.

From CAK, the optical depth of a line in an atmosphere expanding with a radial velocity gradient dV/dr is

$$\tau_L = \frac{\pi e^2}{mc} gf\lambda\left(\frac{N_L}{g_L} - \frac{N_u}{g_u}\right)\left(\frac{dV}{dr}\right)^{-1}. \quad (1)$$

For a rough estimate, we assume a gf-value of unity, a wavelength of 1000 Å, the CAK velocity law of $r^2V(dV/dr) = \frac{1}{2}R_* V_\infty{}^2$, and that the kth element exists only in the jth stage of ionization. Equation (1) becomes

$$\tau_L = 2 \times 10^8 A_k X_L \frac{\dot{M}_{-6}}{(R_*)_{10}(V_\infty)^2_{1000}}, \quad (2)$$

where A_k is the cosmic number abundance of the kth element (normalized to unity), X_L is the population of the Lth level relative to the ion as a whole (1 for resonance lines), and the units are $10^{-6}\ M_\odot\ \mathrm{yr}^{-1}$ for the mass loss rate $\dot{M}$, 1000 km s^{-1} for the terminal velocity V_∞, and 10 $R_\odot$ for the stellar radius R_*. Equation (2) implies that any element whose cosmic abundance exceeds 5×10^{-9} has resonance lines which could potentially be optically thick. In the tabulation of Cameron (1973), there are 27 such elements. Lines arising from excited states are important only in the more abundant elements. For example, in a Boltzmann distribution at $T = 40{,}000$ K, levels of carbon with excitation energies less than 38 eV give rise to subordinate lines which are potentially optically thick. As a second criterion, only lines in the wavelength interval 250–10,000 Å were considered, since a negligible amount of radiative flux is emitted outside this interval by the stars considered here.

The final line list was made by applying these two criteria to the sources of line data given in Table 1. The majority of the gf-values are from the extensive tabulations of Kurucz and Peytremann (1975) and Abbott (1977, 1978*a*), which are theoretical values calculated in the single-configuration approximation. To improve the accuracy of the data, the literature through 1979 was searched for experimental and multiconfiguration transition probabilities. This resulted in the remaining references given in Table 1. (Neutrals were not emphasized in the search, as they are unimportant for the temperatures considered here.)

The line list is complete for the 20 elements of greatest cosmic abundance using the criteria described above. For the remaining 10 elements, some of the ions lack the atomic data needed for the semiempirical calculations of Kurucz and Peytremann. But the ions were not sufficiently abundant to warrant the expense of the *ab initio* calculations of Abbott (1978*a*), and so were neglected.

The summed cosmic abundance of the neglected elements is roughly 10^{-8}, or about $\frac{1}{20}$ that of Mn, the element of smallest abundance for which a complete line list is available. For a wind density of $\dot{M}_{-6}/[(R_*)_{10}(V_\infty)^2_{1000}] = 0.1$, Mn contributes typically 1–2% of the total force with no optically thick lines. For $\dot{M}_{-6}/[(R_*)_{10}(V_\infty)^2_{1000}] = 10$, Mn typically provides 7–8% of the force with roughly 100 optically thick lines. The neglected ions, whose summed abundance is an order of magnitude smaller than Mn, therefore contribute less than 1% of the total force for densities typical of those found in stellar winds.

ii) *Accuracy of the Atomic Data*

Errors in the gf-values propagate through to the calculated acceleration. Most of the important resonance lines from ions of H–Ca have transition probabilities taken from experimental or multiconfigurational calculations, whose quoted uncertainties are of the order 10–20%. The less prominent transitions of the H–Ca ions were calculated mainly from the Coulomb approximation (Abbott 1977). For the example of O IV, these Coulomb approximation values were compared to the more elaborate calculations of Saraph (1980). The ratio $(gf)_{\mathrm{CA}}/(gf)_{\mathrm{Saraph}} = 1.0 \pm 0.6$ for the 130 lines in common, indicating no systematic bias in the Coulomb values, but inaccuracies of typically 60% for a given line.

The gf-values for the iron group ions come solely from single configuration data. Figure 1 shows a comparison between the theory of Abbott (1978*a*) and the lifetime measurements of Anderson, Biemont, and Peterson (1977) and Dumont *et al.* (1979). The discrepancies between theory and experiment are very systematic. First, different transitions within the same ion tend to have roughly the same ratio of theoretical to experimental lifetimes. For example, 11 different transitions of Fe V give a ratio $\tau_{\mathrm{th}}/\tau_{\mathrm{ex}} = 0.6 \pm 0.1$. Second, the discrepancy varies from ion to ion in a manner proportional to the

TABLE 1

SOURCES OF TRANSITION PROBABILITIES

ELEMENT	STAGE OF IONIZATION					
	I	II	III	IV	V	VI
H	48					
He	30	48				
Li	30	30				
Be	30	30	30			
B	30	30, 36	30	30		
C	30, 36, 44	30, 44	11	1, 29		
N	30, 36, 44	30, 44	1, 9, 20, 21, 40	1, 9, 20, 21, 23, 38	1, 8, 9, 18, 20	
O	25, 30, 36	30, 44	1, 32, 34, 39, 42	1, 16, 32, 34, 43	1, 12, 15, 17, 23, 32, 34	1, 5, 29, 34
F	30, 36	25, 30, 44	1, 44	1, 24, 44	1, 41, 44	1, 15, 16, 37, 41
Ne	30	30, 44	1, 14, 22, 27, 44	1, 25, 27, 44	1, 27, 35	1, 25, 27
Na	30	30	1, 3, 19, 47	1	1, 10	1, 10
Mg	30, 36	30, 31	1	1	1	30
Al	30	7, 28, 30	1, 7, 28	1	1	28, 30
Si	30, 36	30, 36, 45	46	26, 30	30	30
P	4, 13, 30	13, 30, 36, 45	13, 30, 36	13, 46	13, 30	30
S	4, 30, 45	30, 44, 45	26, 30, 44, 45	26, 30	26, 46	26, 30
Cl	30, 36	4, 30	30, 44	6, 30	6, 30	46
A	30, 36	26, 30	4, 30, 33	4, 30, 33	26, 30, 33	26, 48
K	30	30	30	4, 30	4, 30	48
Ca	30	30	30	30	4, 30	48
Sc	30	30	30	30	30	
Ti	30	30	30	30	30	
V	30	30	30	30	30	
Cr	30	2, 36	2	2	2	2
Mn	30	30, 36	2	2	2	2
Fe	30	30, 36	2	2	2	2
Co	30	30	30			
Ni	30	30	2	2	2	2
Cu	30	30, 36	30			
Zn	30	30, 36	30			

REFERENCES.—(1) Abbott 1977. (2) Abbott 1978*a*. (3) Anderson *et al.* 1970. (4) Aymar 1973. (5) Barrette *et al.* 1970. (6) Bashkin and Martinson 1971. (7) Baudinet-Robinet, Dumont, and Garnir 1979. (8) Berry *et al.* 1971. (9) Buchet, Poulizac, and Carre 1972. (10) Buchet, Buchet-Poulizac, and Druetta 1978. (11) Castor 1974*b*. (12) Ceyzeriat *et al.* 1970. (13) Curtis, Martinson, and Buchta 1971. (14) Denis 1969. (15) Druetta 1969. (16) Druetta, Poulizac, and Desesquelles 1970. (17) Druetta, Poulizac, and Ceyzeriat 1971. (18) Dufay, Denis, and Desesquelles 1970. (19) Dufay, Gaillard, and Carre 1971. (20) Dumont 1972. (21) Heroux 1967. (22) Hesser 1968. (23) Hummer and Norcross 1974. (24) Irwin and Livingston 1973. (25) Irwin, Livingston, and Kernahan 1973*a*. (26) Irwin, Livingston, and Kernahan 1973*b*. (27) Kernahan, Denis, and Drounin 1971. (28) Kernahan *et al.* 1979. (29) Knystantas *et al.* 1971. (30) Kurucz and Peytremann 1975. (31) Liljeby *et al.* 1980. (32) Lin *et al.* 1972. (33) Livingston, Irwin, and Pinnington 1972. (34) Martinson *et al.* 1971. (35) McIntyre, Donahue, and Bernstein 1978. (36) Morton 1978. (37) Nicolaides, Beck, and Sinanoglu 1973. (38) Nussbaumer 1969*a*. (39) Nussbaumer 1969*b*. (40) Nussbaumer 1971. (41) Nussbaumer and Storey 1979. (42) Pinnington 1970. (43) Saraph 1980. (44) Sinanoglu 1973. (45) Smith 1978. (46) Victor, Stewart, and Laughlin 1976. (47) Westhaus and Sinanoglu 1969. (48) Wiese, Smith, and Glennon 1966.

number of outer shell electrons. A similar behavior was found by Abbott (1978*a*) for discrepancies between the theoretical and experimental energy levels. This suggests that the errors in the theoretical *gf*-values of Figure 1 result from the cumulative effect of many weakly interacting configurations. Even larger uncertainties exist for the lower stages of ionization of the iron group elements, as exemplified by the important ion, Fe II. As summarized most recently by Kurucz (1981), different experimental measures of Fe II oscillator strengths disagree by up to a factor of 2.

To summarize the resonance lines of H–Ca have *gf*-values accurate to 10–20%, while the subordinate lines of H–Ca and all lines of the iron group are uncertain by up to a factor of 2. Changing the *gf*-value of a line has the same effect on the acceleration as changing the abundance of the element. As will be shown in § III*b*, this means that errors in *gf*-values will propagate to the acceleration as the $(1 - \alpha)$ power. As the errors in *gf*-values of different lines from different elements are generally independent, the net uncertainty in the line acceleration, Δa_L, is approximately

$$\Delta a_L = (\Delta E_{gf}/N^{1/2})^{1-\alpha},$$

where N is the number of independent lines and ΔE_{gf} is the uncertainty per line. From the results to be given in § III, typical numbers are $\alpha = \frac{1}{2}$ and $N = 100$, so that assuming $\Delta E_{gf} < 100\%$ means that the uncertainty in the line acceleration because of atomic data is $\Delta a_L < 3\%$. (The temperature range about $T_{\rm eff} = 10{,}000$ K is exceptional. Here the line acceleration is dominated by lines from only one ion, Fe II, so $N = 1$ and $\Delta a_L < 40\%$ may be more appropriate.)

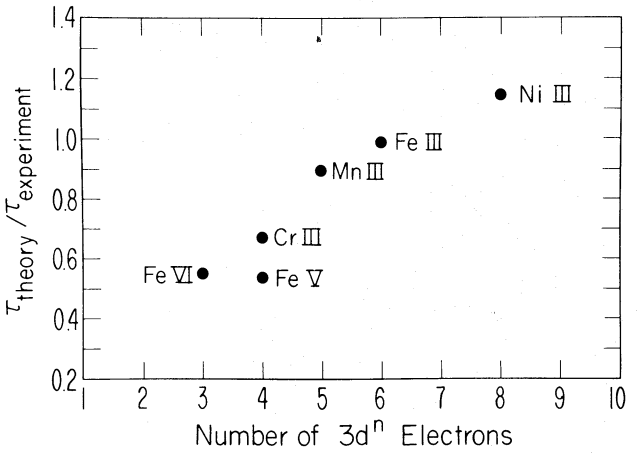

FIG. 1.—A comparison of theoretical and experimental lifetimes for ions of the iron group elements. The ratio of theory to experiment is plotted as a function of the number of outer shell electrons. Each point is an average over several distinct multiplets.

b) *Radiative Transfer*

i) *Basic Equations*

Castor (1974) solved the transfer problem for the line acceleration in a radially expanding atmosphere. As summarized by CAK, the net acceleration by spectral lines is given by

$$a_L = \frac{\sigma_e F}{c} \mathcal{M}(t) , \tag{3}$$

where F is the flux integrated over frequency and σ_e is the electron scattering opacity. The first factor, $\sigma_e F/c$, is the acceleration due to continuum radiation pressure. The contribution of the lines is given by the "force multiplier," $\mathcal{M}(t)$, which is defined by

$$\mathcal{M}(t) = \sum_{\text{lines}} \frac{\Delta\nu_D F_\nu}{F} \frac{1}{t} (1 - e^{-\eta t}) , \tag{4}$$

where F_ν is the emergent flux of the stellar core, $\Delta\nu_D$ is the Doppler width of the line, η is the ratio of line to electron scattering opacity given by

$$\eta = \frac{\pi e^2}{mc} gf \frac{N_L/g_L - N_u/g_u}{\rho\sigma_e \Delta\nu_D} , \tag{5}$$

and t is the optical depth parameter for an expanding atmosphere, defined by

$$t = \frac{\sigma_e \rho V_{th}}{dV/dr} , \tag{6}$$

so that the optical depth of a line in the wind is given by $\tau_L = t\eta$, as stated in equation (1).

As discussed by CAK, equations (4) and (6) are strictly true only in the limit that the stellar photosphere subtends a negligible solid angle at the radius where the line acceleration is being evaluated. At radii close to the photosphere, where the finite angular size of the stellar core is appreciable, the values of the line acceleration given here should be corrected using the formula given by equation (50) of CAK. These corrections will reduce the acceleration by up to 40% near the surface of the star.

The formula for the line acceleration given by equation (4) is accurate to order (V_{th}/V) assuming the following approximations are valid: (1) the velocity law increases monotonically with radius, (2) the scattering is completely noncoherent, (3) the wind is spherically symmetric, and (4) the line source function is given by the theory of Sobolev. The validity of the Sobolev approximation is discussed by Castor (1974), as well as by Paper I. Lucy (1982) interprets recent X-ray observations with a wind model whose velocity law is nonmonotonic. Equation (3) does not apply to such a model.

ii) *The Emergent Flux*

Equations (3) and (4) show that the acceleration is linearly proportional to the radiation flux incident upon the absorbing gas. In this work, as in all previous investigations, the radiation is approximated by the emergent flux from a model atmosphere. This approximation ignores four factors:

1) *The continuum optical depth of the wind.* Observations indicate that the continuum optical depth of the wind is negligible for most OB stars (e.g., Barlow and Cohen 1977). For most Wolf-Rayet stars and a few OB stars of the P Cygni type, continuum optical depth unity occurs at large velocities, and the present wind model is inadequate to represent the radiation field.

2) *Photospheric absorption lines.* Model atmospheres represent only the average continuum flux, and do not include absorption features from individual lines. Yet, at small wind velocities, all lines will absorb radiation emitted from the wings of their own photospheric absorption profiles. In addition, at large velocities, the resonant frequency of a line in the wind may coincide with the photospheric absorption feature of a neighboring line. These effects are neglected in this calculation. However, the next paper in this series will give numerical results for a model which includes this effect.

3) *Line-blanketing.* The model atmospheres of Kurucz (1979) include the effect of line-blanketing in a static atmosphere. However, the opacity of a moving atmosphere is larger by as much as a factor of $V_\infty/V_{th} \sim 100$. Preliminary calculations by Hummer (1981) show that such line-blanketing by the wind causes significant changes in the flux emergent from the stellar core. Such effects are not included in these calculations, but efforts to remedy this defect are under way.

4) *Overlapping lines.* Spectral lines often belong to multiplets, whose wavelength separation is smaller than $\Delta\lambda = \lambda_0 V_\infty/c$, which creates the possibility of overlapping of lines in the wind. Specifically, if a line of rest wavelength λ_0 is moving in the wind at velocity V, it will intercept radiation from the photosphere emitted at wavelength $\lambda_p = \lambda_0(1 - V/c)$. Any line whose rest wavelength λ_0' lies in the interval $\lambda_p < \lambda_0' < \lambda_0$ will also

absorb radiation with wavelength λ_p at a point in the wind whose velocity is given by

$$V' = V - c(1 - \lambda_0'/\lambda_0)\,, \qquad (7)$$

where $V > V' > 0$. The radiation incident to line λ_0 at velocity V depends on the interaction of the radiation and the second line at velocity V'. I call this effect "line overlap," and it adds a velocity dependence to the acceleration.

To estimate the magnitude of line overlap, a test case was computed in the following approximate way. The radiation at line λ_0 was reduced by a factor $\exp[-\sum_i \tau_i(V_i')]$, where the sum is over all intervening lines whose rest wavelengths lie in the interval $\lambda_p < \lambda_i' < \lambda_0$. This is equivalent to assuming that each intervening line absorbs a fraction $(1 - \exp[-\tau_i(V_i')])$ of the incident flux with no reemission of the radiation. Since these lines are resonance lines, which primarily scatter the radiation, this approximation is not realistic. However, it does give a good upper limit to the magnitude of the line overlap effect on the net line acceleration.

c) *Ionization and Excitation*

As described by Mihalas (1978, eq. [5-46]), the ionization equilibrium of these winds can be approximated by

$$\frac{N_J}{N_{J+1}} \approx \frac{1}{2}\left(\frac{h^3}{2\pi mk}\right)^{3/2} \frac{(N_e/W)}{T_R(T_e)^{1/2}} \frac{U_J}{U_{J+1}} \exp\left(\frac{\chi_J}{kT_R}\right), \qquad (8)$$

where W is the dilution factor, χ_J is the ionization potential, U_J is the partition function, and T_R and T_e are the radiation and electron temperatures. Values of T_R versus frequency were taken from the emergent fluxes of the model atmospheres of Kurucz (1979). To estimate the sensitivity of the ionization on the model atmosphere, several test cases were also computed using the models of Mihalas (1972).

The observed ionization balance in OB stars deviates from that predicted from either model, mainly through the presence of trace amounts of highly ionized species such as O VI. Olson and Castor (1981) derived distributions of T_R versus frequency which reproduces the ionization fractions observed in the UV. In all cases, the empirical T_R increases across the He II ionization edge, in contrast to model atmospheres. The effect of this anomalous ionization on the line acceleration was estimated by computing one model with an ionization balance calculated from $T_R(\lambda)$ of the ζ Pup model of Olson and Castor (1981).

The excitation equilibrium was calculated by assuming a Boltzmann distribution at the effective temperature of the star. This is almost certainly in error. Detailed statistical equilibrium calculations find a strong underpopulation of the excited states in expanding atmospheres (e.g., Klein and Castor 1978). The neglect of this effect will be justified *a posteriori* in § IV, which shows that roughly 90% of the acceleration comes from lines arising from ground or metastable states.

III. RESULTS

Conceptually, the line acceleration of equation (3) depends on two factors. The first is the efficiency with which the lines absorb radiative momentum. This efficiency depends on such things as the number of lines, their optical depth, and their distribution with frequency. The second factor is the dynamics of the wind, which enters through the parameter $t \propto \dot{M}/(r^2 V dV/dr)$. Identical distributions of lines will give different values for the line acceleration if the velocity law is different. It is therefore impossible to calculate an absolute value for the line acceleration without simultaneously solving the equation of motion.

This paper is concerned mainly with the efficiency factor—and its dependence on temperature, density, and chemical composition—without wishing to bias the comparison with the uncertainties of any specific hydrodynamic model of the wind. To this end, the line acceleration is tabulated for an assumed grid of t values. By comparing accelerations between models with the same t, but different temperatures, densities, and compositions, one can determine which stars are intrinsically the most efficient at absorbing the radiative momentum.

a) *The Calculated Line Acceleration*

The line acceleration is tabulated in Table 2 in terms of the force multiplier $\mathcal{M}(t)$, defined by equation (4). A model is completely determined by the four parameters $T_{\rm eff}$, log g, N_e/W, and t. The first two parameters, given in columns (1) and (2), specify the model atmosphere of the stellar core. The last two parameters specify the density and dynamics of the absorbing gas, which fixes the line opacity. For each core model, the line acceleration was calculated at a grid of seven decades of t and three densities N_e/W.

The grid of t covers the full range of t which is needed to make a wind model. For $t \lesssim 10^{-7}$, all lines becomes optically thin, and no further increase in $\mathcal{M}(t)$ occurs with decreasing t. For $t \gtrsim 10^{-1}$, the line force becomes negligible compared to the continuum acceleration, and further tabulation is unnecessary.

The grid of N_e/W is spread by a factor of $\pm 10^3$ about a value which is estimated to typify the winds of OB stars. Table 3 lists the parameters of these "typical" models. The parameters represent a horizontal cut in the H-R diagram at a constant luminosity of $M_{\rm bol} = -9$ and constant mass loss rate of $\dot{M} = 1.6 \times 10^{-6}\ M_\odot\ {\rm yr}^{-1}$, which is an estimate from the $\dot{M}$ versus $M_{\rm bol}$ calibration of the radio observations of Abbott, Bieging, and Churchwell (1981*a*). The listed density corresponds to a point in the wind at a radius of $r = 1.5\ R_*$ and velocity $V = V_{\rm esc}$. The exact values chosen are unimportant, as the purpose of Table 3 is merely to provide a center point for the grid of N_e/W. The computed line acceleration was found to be insensitive to the value of log g, so only one gravity was calculated for each $T_{\rm eff}$ to avoid cluttering the tabulated data.

TABLE 2

THE CALCULATED LINE ACCELERATION LOG (Force Multiplier)

				t									
$T_{\rm eff}$ (K)	log g	δ	N_e/W (cm^{-3})	10^{-7}	10^{-6}	10^{-5}	10^{-4}	10^{-3}	10^{-2}	10^{-1}	k	α	σ
6000	0.5	0.16	6.8(+6)	1.478	1.236	0.750	0.316	−0.196	−0.729	−1.291	0.018	0.502	0.055
			6.8(+8)	1.480	1.240	0.761	0.344	−0.129	−0.590	−1.113	0.029	0.465	0.037
			6.8(+11)	2.008	1.911	1.733	1.351	0.854	0.342	−0.263	0.272	0.444	0.123
8000	1.0	0.02	1.7(+6)	2.322	2.045	1.676	1.214	0.687	0.106	−0.553	0.110	0.521	0.079
			1.7(+9)	2.409	2.166	1.778	1.262	0.715	0.127	−0.529	0.105	0.542	0.079
			1.7(+12)	2.581	2.305	1.815	1.294	0.746	0.165	−0.477	0.108	0.555	0.024
10,000	1.5	0.05	3.2(+6)	2.593	2.307	1.961	1.588	1.093	0.482	−0.198	0.288	0.499	0.113
			3.2(+9)	3.000	2.667	2.256	1.818	1.283	0.663	−0.037	0.362	0.538	0.099
			3.2(+12)	3.041	2.690	2.272	1.840	1.301	0.677	−0.026	0.370	0.540	0.102
15,000	2.0	0.12	1.3(+7)	2.525	2.249	1.866	1.296	0.774	0.310	−0.245	0.189	0.505	0.013
			1.3(+10)	2.904	2.468	1.959	1.450	0.922	0.446	−0.096	0.253	0.511	0.020
			1.3(+13)	3.351	2.956	2.555	2.159	1.641	1.034	0.356	0.945	0.517	0.092
20,000	2.5	0.089	3.0(+7)	2.888	2.556	1.965	1.333	0.711	0.266	−0.213	0.140	0.559	0.068
			3.0(+10)	2.976	2.664	2.242	1.702	1.227	0.734	0.124	0.477	0.506	0.035
			3.0(+13)	3.335	2.898	2.406	1.890	1.385	0.873	0.261	0.617	0.523	0.031
30,000	3.5	0.12	1.0(+8)	2.952	2.432	1.857	1.269	0.655	0.109	−0.426	0.093	0.576	0.022
			1.0(+11)	3.289	2.918	2.243	1.523	0.957	0.443	−0.150	0.156	0.609	0.057
			1.0(+14)	3.356	3.032	2.493	1.902	1.379	0.881	0.291	0.571	0.545	0.018
40,000	4.0	0.12	1.8(+8)	3.003	2.737	2.180	1.474	0.770	0.067	−0.639	0.051	0.684	0.041
			1.8(+11)	3.155	2.823	2.292	1.710	1.076	0.452	−0.188	0.174	0.606	0.034
			1.8(+14)	3.355	3.102	2.610	2.026	1.485	0.913	0.228	0.533	0.571	0.046
50,000	4.5	0.092	3.1(+8)	2.970	2.679	2.202	1.590	0.922	0.231	−0.486	0.089	0.640	0.071
			3.1(+11)	3.028	2.785	2.339	1.743	1.106	0.456	−0.199	0.178	0.606	0.062
			3.1(+14)	3.318	3.074	2.635	2.062	1.449	0.845	0.197	0.472	0.582	0.056

CAK developed a formalism in which the force multiplier is approximated by

$$\mathcal{M}(\mathrm{t}) = k\mathrm{t}^{-\alpha}, \qquad (9)$$

where k and α are constants determined by a power law fit to t. An optically thick line has $\alpha = 1$, while an optically thin line has $\alpha = 0$. For each density, values for k and α were computed for the range $10^{-6} \leq \mathrm{t} \leq 10^{-1}$. The standard deviation of the analytic approximation of equation (9) from the exact values of Table 2 is given by σ in the last column of Table 2. The power law fit is typically accurate to ± 0.05 dex.

b) *The Dependence of the Line Acceleration on Stellar and Wind Properties*

As discussed above, the dependence on temperature, density, and composition is determined by keeping t fixed and varying the other parameters individually. One minor complication affecting the comparison with temperature and composition is that these parameters enter the force multiplier both explicitly through the calculated values of k and α, and implicitly through the definition of $\mathrm{t} \propto \sigma_e V_{\rm th}$.

Consider first the temperature dependence, which enters the formula for the line acceleration through the quantities: $\Delta v_{\rm D} \propto V_{\rm th}$, $\mathrm{t} \propto V_{\rm th}$, and $\eta \propto V_{\rm th}^{-1}$. From equations (4), all of these dependences cancel in the net value for the acceleration; i.e., *the line acceleration from a single line is independent of the thermal velocity*. The choice of a formula for $V_{\rm th}$ in the computation of t and $\mathcal{M}(\mathrm{t})$ is therefore completely arbitrary. The definition $V_{\rm th} \equiv [2kT_{\rm eff}/m_{\rm H}]^{1/2}$ has been used throughout this work.

Now consider the case of two winds with two different adopted values for $V_{\rm th}$, but exactly the same number and

TABLE 3

PARAMETERS OF THE CALCULATED MODELS

$T_{\rm eff}$ (K)	$M/M_\odot$	$R/R_\odot$	log g	Γ	$V_{\rm esc}$ (km s^{-1})	N_e/W (cm^{-3})
50,000	50	8	4.4	0.16	1400	3.3(+11)
40,000	40	12	3.9	0.20	1000	1.9(+11)
30,000	30	22	3.2	0.29	600	1.0(+11)
20,000	30	48	2.5	0.29	400	3.0(+10)
15,000	30	86	2.0	0.29	300	1.3(+10)
10,000	30	190	1.3	0.29	200	3.8(+9)
8000	30	300	0.9	0.29	160	1.9(+9)
6000	30	540	0.4	0.29	120	8.2(+8)

distribution of lines. The contribution of the optically thick lines to the force multiplier as a function of t is

$$\mathcal{M}_{\rm thick} = \sum_{\rm thick} \frac{\Delta\nu_{\rm D} F_\nu}{F} \frac{1}{\rm t} \propto \frac{V_{\rm th}}{\rm t} . \qquad (10)$$

The contribution of the optically thin lines is

$$\mathcal{M}_{\rm thin} = \sum_{\rm thin} \eta \frac{\Delta\nu_{\rm D} F_\nu}{F} \neq f(V_{\rm th}, {\rm t}) . \qquad (11)$$

When comparing winds with the same assumed value of t, equation (10) shows that the optically thick lines create an apparent dependence on $V_{\rm th}$. To properly determine the dependence of the line acceleration on temperature, one must therefore compare the values of the quantity $(V_{\rm th})^{-\alpha}\mathcal{M}({\rm t})$ for models with the same t but different $T_{\rm eff}$.

Likewise, the dependence of the line acceleration on chemical composition cannot be determined by simply comparing values of the force multiplier for the same t, but different abundances. This is because the parameter σ_e enters both the definition of t and the proportionality between a_L and $\mathcal{M}({\rm t})$. An analysis similar to that for $V_{\rm th}$ shows that the relevant quantity to isolate the dependence on composition is $(\sigma_e)^{1-\alpha}\mathcal{M}({\rm t})$.

i) *Dependence on Density*

The line acceleration depends on density in two ways. First, the atoms which absorb radiation over a frequency interval $\Delta\nu_{\rm D}$ have a mass per unit area of $\rho V_{\rm th}(dV/dr)$. The line force per unit mass is therefore inversely proportional to ρ. This direct dependence of a_L on ρ is accounted for by the parameter t.

The density also enters the line acceleration indirectly through the dependence of the ionization balance on electron density, as shown by equation (8). The higher the density, the lower the overall state of ionization. Since the lower stages of ionization have more lines, which are usually nearer the maximum of the emergent flux, the acceleration generally increases with increasing density. For each $(T_{\rm eff}, g)$, a power law fit was performed for the three calculated values of N_e/W, to give $\mathcal{M} \propto N_e^{\delta}$. The value of the constant δ is given in column (3) of Table 2.

The dependence of the line acceleration on density is illustrated in Figure 2*a* for three representative values of t and temperatures in the range $50{,}000 \geq T_{\rm eff} \geq 10{,}000$ K. The density dependence is similar for all temperatures. For a given $T_{\rm eff}$, the line acceleration may increase in a discontinuous manner with density, but averaging over all temperatures and densities, there is a smooth increase as indicated by the dashed lines. These lines are least squares fits, all of which have a slope of $\delta = 0.09$. The scatter about the mean fits is roughly 0.2 dex, with no temperature consistently above or below the mean relation.

ii) *Dependence on Effective Temperature*

As shown above in Figure 2*a*, the force multiplier is remarkably independent of $T_{\rm eff}$ over the range $50{,}000 \geq T_{\rm eff} \geq 10{,}000$ K. To more clearly define the temperature

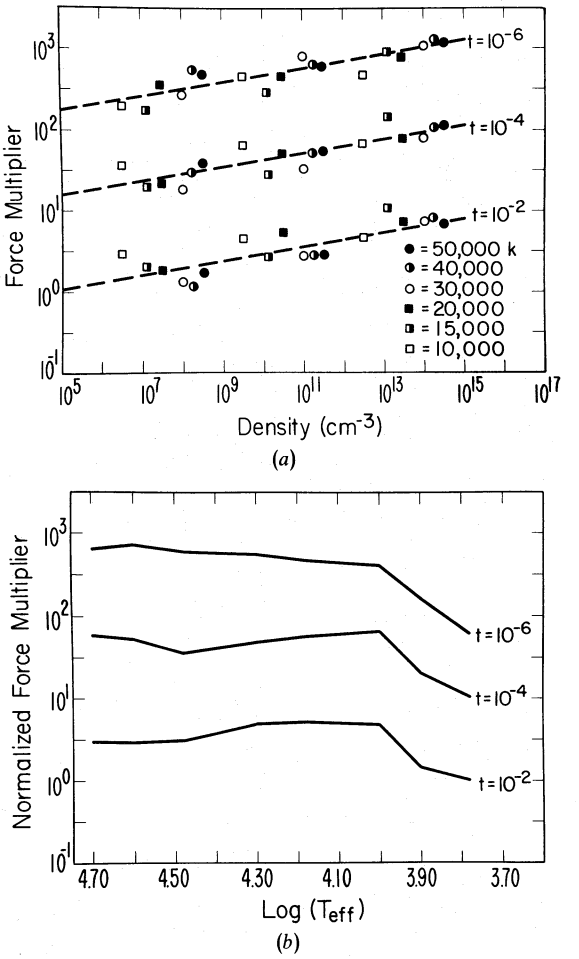

FIG. 2.—(*a*) The dependence of the line acceleration on the density of the absorbing gas in the wind for three representative values of t. N_e/W is the electron density divided by the dilution factor, which is the effective density of the wind entering the equation for the ionization balance. The dashed lines are least squares fits, which all have a slope of 0.09. The acceleration increases with density because a lower degree of ionization is more favorable for radiative acceleration. (*b*) The dependence of the line acceleration on effective temperature for the same three values of t. The force multiplier from different models has been normalized to the common density $N_e/W = 10^{11}$ cm^{-3}. The acceleration is remarkably insensitive to temperature.

dependence, different models must be compared at the same density. Averaging the data of Table 2 over density and then scaling to a common density of $N_e/W = 10^{11}$ cm^{-3} gives the normalized force multiplier displayed in Figure 2*b*. Over the temperature range $50{,}000 \geq T_{\rm eff} \geq 10{,}000$ K the force multiplier is essentially constant. The force multiplier is smaller by roughly 0.4 dex at $T_{\rm eff} = 8000$ K, and 0.7 dex at $T_{\rm eff} = 6000$ K.

Combining the results of the data in Figures 2*a* and 2*b*, the force multiplier is given to within a factor of 2 accuracy over the temperature range $50{,}000 \geq T_{\rm eff} \geq 10{,}000$ K by the single expression

$$\mathcal{M}({\rm t}) = 0.28{\rm t}^{-0.56}(N_{11})^{0.09} , \qquad (12)$$

i.e., $\bar{k} = 0.28$, $\bar{\alpha} = 0.56$, $\bar{\delta} = 0.09$, and N_{11} is N_e/W in units of 10^{11} cm^{-3}. Equation (12) is probably sufficiently accurate for most applications of these data. While the force multiplier is sharply reduced at temperatures cooler than 10,000 K, it is still significantly above unity, indicating that radiation forces may be important even in the F and G supergiants.

As discussed in the beginning of this section, if k and α are constant with $T_{\rm eff}$ for the same t, this implies an increase in the efficiency of line absorption by a factor $V_{\rm th}^{-\alpha}$, or $T_{\rm eff}^{-\alpha/2}$, for the range 50,000 $\geq T_{\rm eff} \geq$ 10,000 K. An A0 star therefore has nearly twice as many effective lines absorbing the radiation flux as an O4 star with the same wind density and velocity structure.

iii) *Dependence on Chemical Composition*

Two kinds of variation in chemical composition were considered. In the first case, the abundance of all elements heavier than H and He was multiplied by a constant factor. This approximates differences in the initial stellar composition of stars of different population types or galactic location. In the second case, the initial composition was enriched by the products of nuclear burning, which is relevant to the problem of mass loss by Wolf-Rayet stars.

Variations in metallicity. Two models were computed, one with a metallicity of three times solar and one with a metallicity of one-third solar. The results are shown in Figure 3*a* for a density of $N_e/W = 1.8 \times 10^{11}$ cm^{-3}. For comparison the solid line shows the acceleration using solar abundances from Cameron (1973). All three models used an emergent flux from the stellar core from a (40,000 K, 4.0) model of Kurucz (1979). This neglects differences in the emergent flux that might occur because of variations in metallicity.

The data for the three models are well fitted by the relation $a_L \propto Z^{0.4}$. This is exactly what is expected from the scaling law suggested by CAK of $a_L \propto Z^{(1-\alpha)}$. The dependence is less than linear, because increasing the opacity of lines which are already optically thick does not increase the line acceleration.

Enrichment by nuclear burning. The WN and WC sequences of Wolf-Rayet stars are stars whose chemical composition presumably reflects the products of

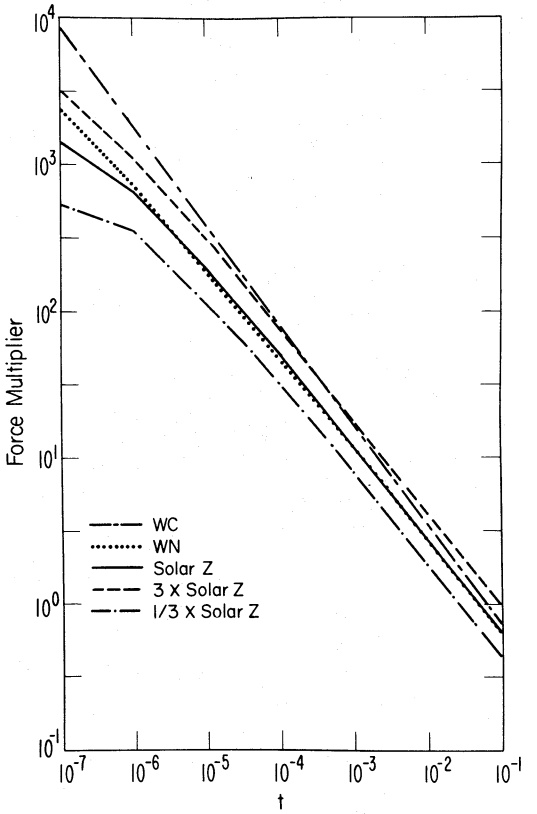

FIG. 3*a*

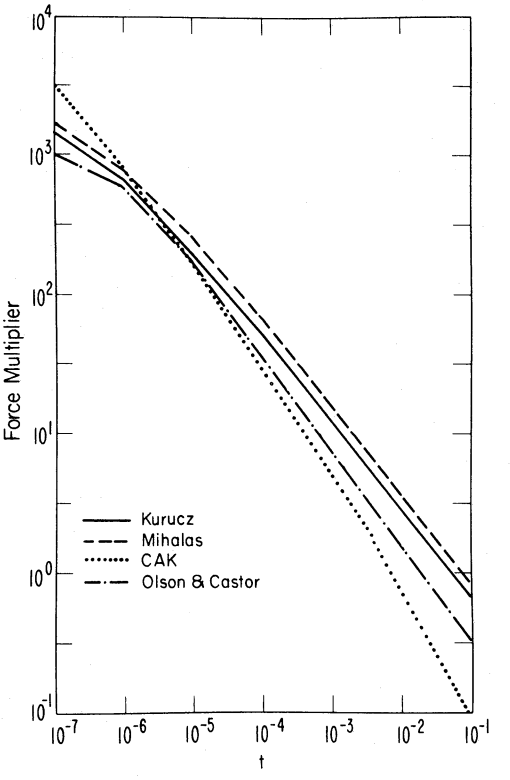

FIG. 3*b*

FIG. 3.—(*a*) The dependence of the line acceleration on chemical composition. In all cases the core model atmospheres had $T_{\rm eff}$ = 40,000 K, log g = 4.0, and solar composition. The five cases shown all had different compositions for the absorbing gas in the wind, which are described in the text. The acceleration increases with increasing mass fraction of metals in the wind. (*b*) The dependence of the line acceleration on the ionization balance in the wind. Again, the core model atmosphere had $T_{\rm eff}$ = 40,000 K, log g = 4.0, and solar composition. The model using observed ionization fractions gives less acceleration than either radiative equilibrium model, but the differences are small. For comparison, the dotted line shows the line acceleration computed by CAK from the C III ion.

hydrogen and helium burning, respectively (e.g., Conti 1982). Two test cases were computed. The first model represents a star which has exhausted its hydrogen but has not yet burned helium. The number abundances of CNO are $[C/He] = 2.7 \times 10^{-4}$, $[N/He] = 1.0 \times 10^{-2}$, and $[O/He] = 2.3 \times 10^{-4}$, as calculated by Vanbeveren and Doom (1980). The mass fractions of all other elements are unchanged. This model is appropriate for stars in the WN sequence, although WN stars typically have abundances intermediate between solar and complete hydrogen exhaustion.

The second model represents a star which has exhausted its helium, but not yet processed any heavier elements. The assumed abundances are zero hydrogen, helium, or nitrogen, and mass fractions for the enhanced elements of C = 0.27, O = 0.71, and Ne = 0.024. The mass fractions of all other elements are unchanged. This composition comes from a model calculated by Lamb, Iben, and Howard (1976), and it provides an upper limit to the composition changes expected of stars in the WC sequence.

The line acceleration from these models is compared to the solar case in Figure 3*a*. The quantity plotted is $[(\sigma_e)_{WR}/(\sigma_e)_{solar}]^{1-\alpha}\mathcal{M}(t)$ because, as discussed at the beginning of this section, this quantity gives the true comparison of the efficiency of line acceleration between models of different chemical composition. The scaled line acceleration of the WN case is virtually identical to that of the solar case. This is expected, because neither hydrogen nor helium contributes significantly to the line acceleration, so converting hydrogen into helium leaves the acceleration unchanged. Some small differences do exist between these two models, because of the rearrangement of mass among C, N, and O. The line acceleration of the WC case is larger than solar by up to a factor of 2. This is a smaller increase than predicted by the $a_L \propto Z^{1-\alpha}$ relation derived above, which predicts roughly a factor of 3 increase for a factor of 50 increase in Z and $\alpha = 0.7$ for the WC model. The reason for the discrepancy is that the increase in metallicity is concentrated in only two elements in the WC case. There is a limit as to how many lines an individual element can have at a frequency near the maximum of the emitted flux. Once all of these lines become optically thick, further increases in abundance do not produce any further increase in the line acceleration.

iv) *Dependence on Ionization*

The adopted ionization balance is an area of uncertainty in these calculations. First, even assuming radiative equilibrium, the fluxes from different model atmospheres of the stellar core will give different states of ionization in the wind. Second, the ionization states observed in the wind do not match the predictions from any model atmosphere. As described in § IIc, three test cases were computed to determine the sensitivity of the line acceleration to the ionization state of the wind. All used emergent fluxes from a model atmosphere with $T_{eff} = 40{,}000$ K and $\log g = 4.0$. The first two cases compare states of ionization calculated from color temperatures of the model atmospheres of Kurucz (1979) and Mihalas (1972). The ionization balance of the third case is based on empirical ionization fractions determined by Olson and Castor (1981) from UV observations of the star ζ Pup.

The line acceleration from the three models is compared in Figure 3*b*. The Mihalas models have a line acceleration that is ~25% larger than that of the Kurucz models. This difference is almost entirely due to the ionization balance, as differences in the emergent flux with wavelength tend to even out when summed over all lines. The line acceleration using empirical ionization fractions is a factor of ~2 smaller than a model calculated using the ionization from the Mihalas model, but identical emergent fluxes.

The relationship of ionization balance to line acceleration is shown by comparing the relative contributions of the oxygen ions to the acceleration. As shown by Table 4, the Kurucz model gives an ionization balance that is much more sharply peaked about the dominant stage than that of the Mihalas model. The contribution of O IV to the force is about the same for the two cases, but that of O III and O V is down by a factor of 2 in the Kurucz model, giving a net reduction of ~20% in the line acceleration from oxygen.

The empirical ionization balance of oxygen appears favorable for line acceleration, because there are two dominant states of ionization rather than one. The net gain in absorbing lines is actually smaller, however, because the higher stages of ionization have both fewer lines and lines that are at shorter wavelengths, where less flux is emitted. Thus, the large reduction in O III abundance and small reduction in O IV abundance more than offsets the gain on the O V lines. The net result is a factor of 2 decrease in the line acceleration of the empirical case over that of the Mihalas model.

Highly ionized species, such as O VI, are also observed in OB stars as a result of the X-ray flux emitted by the wind (e.g., Cassinelli *et al.* 1981). The presence of O VI, or other anomalously high stages of ionization, has a negligible impact on the net line acceleration for two reasons: (1) they are only present in trace amounts (typically 10^{-3} to 10^{-4} of the total

TABLE 4

A COMPARISON OF THE LINE ACCELERATION FROM OXYGEN FOR THREE DIFFERENT MODELS OF THE IONIZATION BALANCE

Model	Ion Fractions of Oxygen			Force Multiplier from Oxygen Lines ($t = 10^{-4}$)
	O III	O IV	O V	
Mihalas	0.04	0.95	0.006	20.9
Kurucz	0.02	0.98	0.003	16.3
Empirical.....	0.0003	0.63	0.37	10.7

NOTE.—All three models were parameterized by $T_{eff} = 40{,}000$ K, $\log g = 4.0$, and $N_e/W = 1.8 \times 10^{11}$ cm^{-3}.

number abundance of the element), and (2) they have, at most, one strong line at frequencies where the radiative flux is emitted.

c) *The Identity of the Accelerating Lines*

In addition to the total value of the line acceleration, it is also of interest to determine (1) which individual lines are providing the most force, (2) from which spectral regions most of the radiative momentum is being absorbed, and (3) how many lines are required to accurately calculate the line acceleration. The answer to the third question is dependent on the value of the parameter t. Figure 4 shows the percentage contribution to the line acceleration as a function of the number of lines included in the computation, where the lines are ordered by the magnitude of their line acceleration.

For small values of t, the force is given to good accuracy by a list of several hundred of the most important lines. For large values of t, several thousand lines are required. To understand this difference, consider two lines, one a resonance line with close to the maximum opacity possible, $\eta_R \approx 10^7$, and the other a neighboring weaker line with only 100 times the continuum opacity $\eta_w \approx 10^2$. If $t = 10^{-2}$, both lines contribute equally to the acceleration. If $t = 10^{-7}$, the weak line contributes less than the strong one by a factor of 10^5. Once t becomes small enough to desaturate the strongest lines, those lines will dominate the force. Small values of t are characteristic of small mass loss rates and/or steep accelerations. Larger values of t occur in regions of the wind where the acceleration is very gradual.

This reasoning also explains the differences between these calculations and those of CAK, who approximated the true distribution of lines by the lines of C III at a cosmic abundance of 10^{-3}. Figure 3*b* compares the CAK force multiplier to the model of Table 2 for a temperature of 40,000 K. At the larger values of t, CAK is too small, because it does not account for the contribution of the very numerous lines of the heavier metals. For $t \lesssim 10^{-6}$, CAK becomes larger, because its strongest resonance lines are still optically thick as a result of their artificially large cosmic abundance. The slope of the line in Figure 3*b*, which is parameterized by α, is always smaller in the realistic case than in the calculations by CAK, which dramatically alters the predicted behavior of $\dot{M}$ and V_∞.

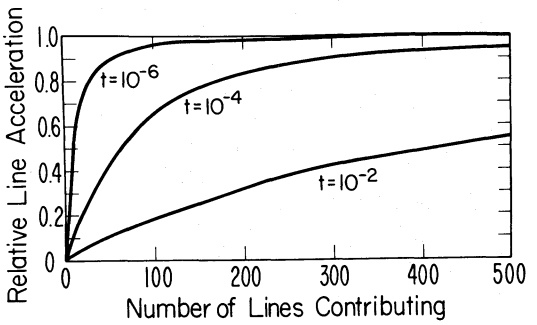

FIG. 4.—The number of lines required to give an accurate representation of the line acceleration. The plot shows the fraction of the total line acceleration provided by the number of lines indicated on the horizontal axis. The lines were ordered by the size of their contribution to the acceleration. Good accuracy is typically assured by a calculation which includes several thousand of the most important lines.

A second question is: Which elements are contributing most of the force? Figure 5*a* shows the percentage contribution to the line acceleration by four different groups of elements for $t = 10^{-4}$ and the models of Table 3. The large contribution of Fe II to the line acceleration is very evident for $T_{\rm eff} = 10{,}000$ K. Otherwise, no single element dominates the acceleration at any temperature. Although H and He are the most abundant elements, they contribute negligibly to the acceleration.

Figure 5*b* shows which spectral region is providing the radiative acceleration. For $T_{\rm eff} \geq 40{,}000$ K, over 80% of the acceleration arises from lines in the Lyman continuum, which are not observable. These models are therefore very sensitive to the estimated emergent flux in the Lyman continuum, which is uncertain in the model atmospheres. In the late O and early B supergiants, most of the acceleration comes from lines in the Balmer continuum, so these stars provide a better opportunity to test theory and observation.

For all stars, roughly half the line acceleration is provided by optically thick lines. The remaining contribution comes from a larger number of optically thin lines. This is consistent with values of $\alpha = 0.5$–0.6 derived from power law fits to $\mathcal{M}(t)$ in Table 2. About half the acceleration therefore comes from lines which are not opaque enough to have pronounced, violet-shifted, absorption profiles.

Over 80% of the acceleration comes from lines whose lower levels are either a ground or metastable state. Excited states with allowed radiative transitions to lower states are strongly underpopulated in an expanding atmosphere. From Figure 5*b*, this effect pertains to only 10–20% of the tabulated acceleration, so the error is small.

All of the above features of the line acceleration are illustrated by Table 5, which gives a list of the 15 lines at each $T_{\rm eff}$ which contribute the most to the acceleration. The optical depth given in Table 5 is the expansion optical depth, $\tau_L = \eta t$, computed for $t = 10^{-4}$. Also given is the value of the force multiplier contributed by each line, $\mathcal{M}(t = 10^{-4})$. The lines with the most acceleration are not usually the strongest lines in optical depth. Typically, all spectral regions are well blanketed by lines, and the most important lines are therefore those that happen to lie at the frequency where νF_ν is a maximum. Since νF_ν is larger as $T_{\rm eff}$ increases, the acceleration per line is also larger in the hotter stars. To achieve the same total acceleration, the cooler stars have more lines situated where the flux is significant.

Lucy and Solomon (1970) approximated the line acceleration using the strongest resonance lines of a few prominent elements. CAK emphasized the importance of many weaker lines to the total force, which they approximated using many subordinate lines of C III. The

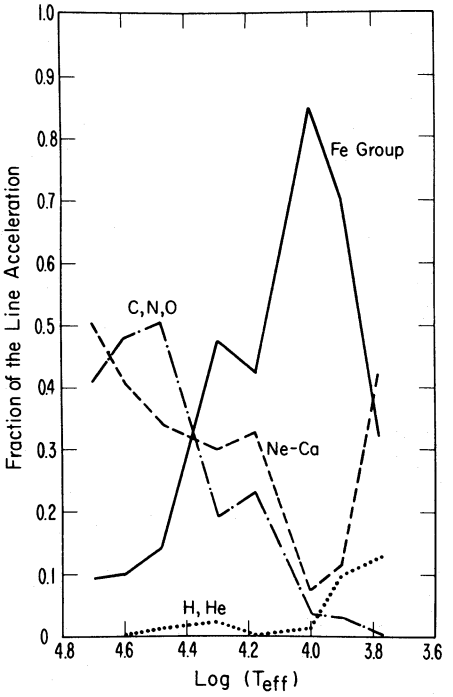

FIG. 5a

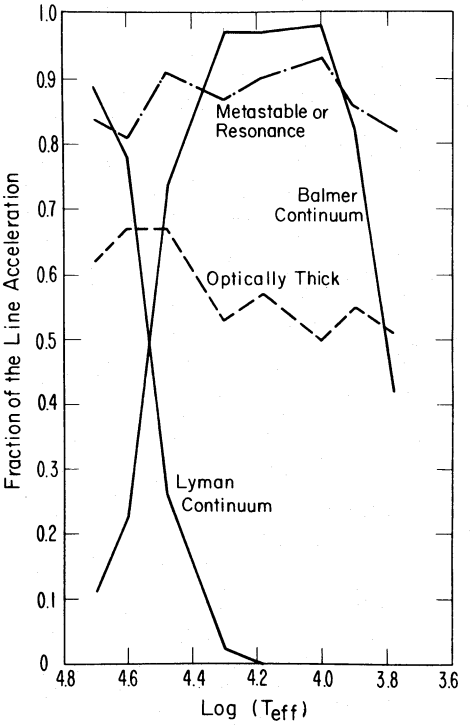

FIG. 5b

FIG. 5.—(*a*) The fraction of the total line acceleration provided by lines from the elements: (i) H and He, (ii) C, N, and O, (iii) Ne through Ca, and (iv) Cr, Mn, Fe, and Ni. The acceleration is provided almost entirely by metals. (*b*) The fraction of the total line acceleration which is provided by lines: (*i*) with wavelengths in the Lyman and Balmer continua, (ii) which are optically thick in the wind, and (iii) whose lower levels are either ground or metastable states.

true answer is that the line force is dominated by a very large number of resonance or metastable lines from many elements.

A striking feature of Table 5 is that the lines tend to be distributed in wavelength in a clumpy manner. Most of the force comes from multiplets which typically have half a dozen individual lines. In the calculations presented in Table 2, two lines were treated as distinct if the separation of their rest wavelengths exceeded the sum of their Doppler widths. In reality, these lines will interact because their velocity-shifted wavelengths overlap in the wind. Table 5 emphasizes that the problem of overlapping lines in the wind must be dealt with to make future improvements to the calculated values of the line acceleration.

d) *Overlapping Lines*

The dependence of the line acceleration on line overlap is shown in Figure 6. As described in § II*b*, at high wind velocities the red component of two closely spaced lines is Doppler-shifted to wavelengths where the radiation flux has already interacted with the blue component. A fraction $(1 - e^{-\tau_B})$ of the line acceleration provided by the red component therefore suffers from the uncertainty of line overlap, where τ_B is the optical depth of the blue component. By definition, there is no line overlap for wind velocities less than V_{th}. Between $1 \lesssim V/V_{th} \lesssim 50$, line overlap occurs between fine structure components of most multiplets, and the fraction of the total line acceleration which suffers from line overlap increases dramatically. For $V/V_{th} \gtrsim 50$, line overlap occurs mainly between two distinct multiplets, which is relatively rare because of their large average wavelength separation, so the dependence of the acceleration on line overlap increases much more slowly with increasing velocity. Line overlap also increases with increasing t, because the larger the value of t, the greater is the total number of optically thick lines, which enhances the probability that two lines overlap.

Exact calculations of the line acceleration from overlapping doublets (Olson 1982) and overlapping lines with a stochastic distribution of frequencies (Castor 1979) show that line overlap can either increase or decrease the acceleration, depending on the optical depth of the line, the velocity law, and the separation of the rest frequencies. In most instances, the acceleration is reduced at small radii and enhanced at large radii. Thus, the present calculations probably give the correct answer for some sort of mean value of the line acceleration. However, to solve the hydrodynamic equations properly, one must consider the gradients in the line acceleration with radius which are caused by a line overlap.

e) *Flux Blocking*

The main features of the line acceleration are summarized in the plots of Figure 7, which show the

TABLE 5

LINES WHICH CONTRIBUTE THE LARGEST RADIATIVE ACCELERATION AT $t = 10^{-4}$

Ion	λ(Å)	$\tau_L(t = 10^{-4})$	$\mathcal{M}(t = 10^{-4})$	Type[a]
$T_{\rm eff}$ = 6000 K, log g = 0.5, $N_e/W = 6.8 \times 10^8$ cm^{-3}				
H I	6562.82	1.7	0.20	S
Ca II	8542.09	3.7	0.19	M
Ca II	8542.22	3.7	0.19	M
Ca II	8662.14	2.1	0.17	M
Ca II	3968.47	96.7	0.10	R
Ca II	8497.99	0.4	0.07	M
Ca II	3933.66	197.3	0.06	R
H I	4861.22	0.2	0.05	S
Ca II	3736.90	0.2	0.02	S
Fe II	2984.82	2.1	0.02	M
Ca II	3179.33	0.8	0.02	S
Ca II	3179.37	0.8	0.02	S
H I	4340.46	0.1	0.02	S
Ti II	3759.29	0.1	0.02	M
Ti II	3349.40	0.4	0.01	R
$T_{\rm eff}$ = 10,000 K, log g = 1.5, $N_e/W = 3.2 \times 10^9$ cm^{-3}				
H I	4101.69	43.2	0.38	S
H I	4340.45	91.5	0.34	S
H I	4861.22	269.8	0.28	S
Fe II	2984.82	4.2	0.19	M
Mg II	2936.50	5.6	0.19	S
Mg II	2928.63	2.8	0.18	S
Mg II	2802.69	793.0	0.17	R
Mg II	2798.81	25.1	0.16	S
Fe II	2714.38	4.1	0.16	M
Fe II	2631.32	23.1	0.16	R
Fe II	2631.05	24.5	0.16	R
Fe II	2727.54	4.3	0.16	M
Fe II	2739.51	21.8	0.16	M
Fe II	2743.18	8.2	0.16	M
Fe II	2746.48	13.4	0.16	M
$T_{\rm eff}$ = 20,000 K, log g = 2.5, $N_e/W = 3.0 \times 10^{10}$ cm^{-3}				
Si III	1294.53	10.3	0.59	M
Si III	1296.73	8.4	0.58	M
Si III	1298.92	30.4	0.58	M
Si III	1298.89	6.2	0.58	M
Si III	1301.10	8.4	0.57	M
C II	1335.66	6.0	0.57	R
Si III	1303.29	10.2	0.57	M
C III	1247.38	2.6	0.57	S
C II	1334.51	3.0	0.54	R
Fe III	1122.53	4.0	0.49	R
C III	1174.98	59.0	0.48	M
Si III	1113.23	46.9	0.48	M
C III	1175.40	47.2	0.48	M
Si III	1113.20	8.5	0.48	M
C III	1175.62	185.6	0.48	M
$T_{\rm eff}$ = 40,000 K, log g = 4.0, $N_e/W = 1.8 \times 10^{11}$ cm^{-3}				
N IV	955.29	3.2	0.82	S
S VI	944.50	3.8	0.78	R
Ar V	949.38	2.0	0.70	M
S VI	933.37	7.5	0.68	R
N V	1238.80	3.6	0.61	R
N IV	924.25	17.5	0.57	M
N IV	923.67	14.6	0.56	M
N IV	922.52	14.6	0.55	M
N IV	921.95	17.5	0.54	M
P V	1117.99	1.2	0.52	R
N V	1242.77	1.8	0.52	R
O IV	790.20	350.7	0.43	R
O IV	790.10	39.3	0.43	R
O IV	787.71	190.7	0.43	R

[a] R = Resonance line. M = Subordinate line arising from a metastable level. S = Subordinate line arising from a level with allowed downward radiative transitions.

blocking of the emergent flux by lines in the expanding envelope. The shaded regions show the wavelength intervals where momentum is being transferred from the radiation to the wind. Figure 7 was made using the models of Table 3 and $t = 10^{-3}$. For each line the relative flux, vF_v/F, emergent from the model atmosphere was multiplied by $e^{-\tau_L}$ over a wavelength interval $\lambda_0(1 - V_\infty/c) \leq \lambda \leq \lambda_0$, where λ_0 is the rest wavelength of the line and $\tau_L = \eta t$. The adopted terminal velocities were $V_\infty = 3V_{\rm esc}$ for $50{,}000 \geq T_{\rm eff} \geq 30{,}000$ K, $V_\infty = 2V_{\rm esc}$ for $T_{\rm eff} = 20{,}000$ K, and $V_\infty = V_{\rm esc}$ for $T_{\rm eff} = 10{,}000$ K (cf. Fig. 9). The purpose of Figure 7 is to show those frequency intervals where radiative momentum is being absorbed by the lines. The plots do not resemble the flux observed from OB stars because: (1) reemission of radiation absorbed by the lines is not accounted for, and

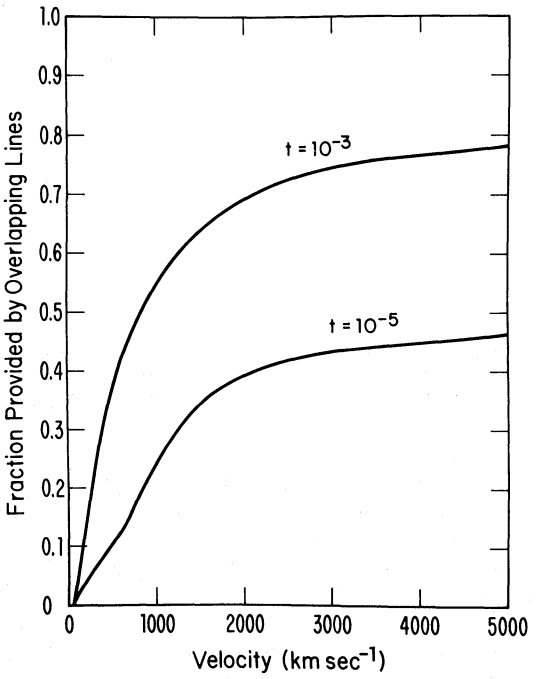

FIG. 6.—The fraction of the total line acceleration provided by lines whose Doppler-shifted frequencies overlap with that of a neighboring line at shorter wavelengths. The higher the wind velocity, the more lines overlap. This model had a core atmosphere with $T_{\rm eff}$ = 40,000 K and log g = 3.5.

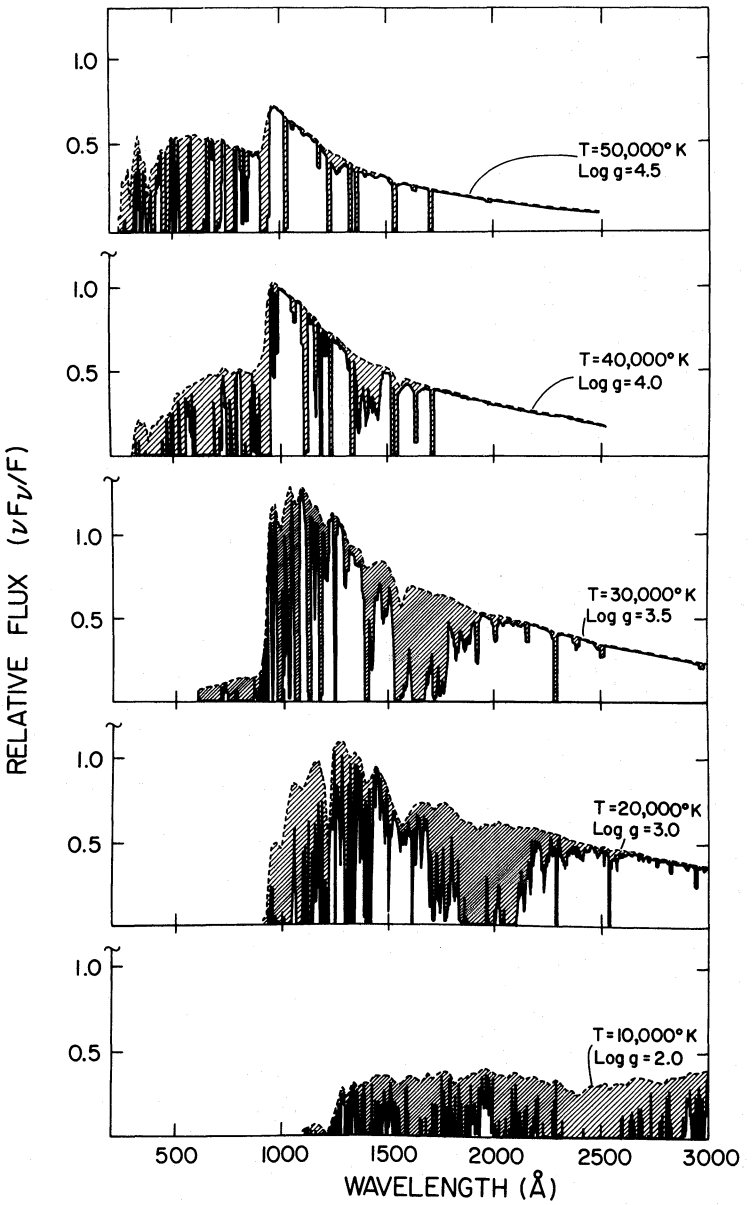

FIG. 7.—Line blocking of the emergent flux by the wind. Dashed lines show the emergent flux from the indicated model atmosphere of Kurucz (1979). Shaded areas show wavelengths where the momentum of the radiation field is absorbed by the wind. For the purpose of illustration, all models were calculated for $t = 10^{-3}$, which corresponds to an unusually high wind density. The fraction of the flux which is blocked by lines is nearly constant over the temperature range 50,000 K $\geq T_{\rm eff} \geq$ 10,000 K.

(2) for the purpose of illustration, the plots use an unusually large value of $t = 10^{-3}$, which corresponds to a mass loss rate of $\sim 10^{-5}\ M_\odot\ {\rm yr}^{-1}$.

A primary result of this paper is that, over the entire temperature range 50,000 $\geq T_{\rm eff} \geq$ 10,000 K, the line acceleration can be represented by a single analytic expression, equation (12). Figure 7 shows the reason for this constancy. For a given temperature, the prominent lines tend to fall at or near the maximum momentum of the radiation field, which is proportional to νF_ν. The coincidence of the lines with the radiation maximum is not accidental, because the radiation field determines the ionization balance. For densities typical of those in the winds of OB stars, the dominent state of an element has an ionization energy of $I \sim 20$–$30kT$. Resonance lines from the dominant stage of ionization typically lie at wavelengths corresponding to roughly $I/4$, or, 5–$7kT$. The maximum in the function νB_ν is $4kT$. Therefore, the absorbing lines are located at, or somewhat above, the frequency of the maximum of the radiation field.

For temperatures smaller than $T_{\rm eff} = 10{,}000$ K, the maximum of the radiation field moves into the Paschen continuum. The wavelengths of the dominant lines no longer follows the maximum of the radiation field,

because even for neutrals most resonance lines lie in the Balmer continuum. Thus, the line acceleration drops off sharply for $T_{\rm eff} < 10{,}000$ K, which is what the detailed results of Table 2 showed.

The above reasoning also explains why the line acceleration decreases with increasing degree of ionization. Even for the case of radiative equilibrium, with no mechanical heating, the prominent lines tend to be concentrated at or above the frequency of the maximum of vF_v. Any increase in the degree of ionization will shift the wavelength of the absorbing lines to yet higher energies, even further from the wavelength of the radiation maximum. For example, it is easy to see from Figure 7 that little or no radiation from the $T_{\rm eff} = 30{,}000$ K model would be absorbed by lines whose ionization state was given by the $T_{\rm eff} = 50{,}000$ model. Since the lower stages of ionization generally have a greater number of lines, this effect becomes even larger.

Figure 7 shows that flux blocking by lines in the wind becomes very significant for high rates of mass loss. Hummer (1981) estimates that the continuum radiation field is significantly altered when more than 10% of the emergent continuum flux is scattered back onto the stellar core by lines in the wind. Each line backscatters a fraction $W(1 - e^{-\tau_L})$ of the radiation, so the total fraction of the radiation reflected on to the core by the wind is

$$f = \sum_i \int_0^{V_\infty} dV W \frac{\nu_0 {}^i F_{\nu_i}}{cF} (1 - e^{-\tau_L}) . \qquad (13)$$

Evaluating equation (13) with the velocity law $V = V_\infty(1 - R_*/r)^{1/2}$, and with the definition and numerical value of $\mathcal{M}(t)$ from equations (4) and (12), the wind reflectance becomes

$$f = 0.2 \frac{V_\infty t}{V_{\rm th}} \mathcal{M}(t) \approx 0.056 \frac{V_\infty}{V_{\rm th}} t^{0.44} . \qquad (14)$$

Line blanketing by the wind therefore becomes significant for $t \gtrsim 10^{-4}$ for a ratio $V_\infty/V_{\rm th} = 100$, which is typical of O and early B stars. This corresponds to a threshold mass loss rate of $\sim 10^{-6}\ M_\odot\ {\rm yr}^{-1}$.

IV. COMPARISON TO OBSERVATION

This section compares the observed mass loss rates and terminal velocities to those predicted by the wind theory of CAK using the line acceleration of this paper. The line acceleration is accurate to within a factor of 2 or 3, as discussed in the previous section. The predicted values of $\dot{M}$ and V_∞ may not match this accuracy, if the solution to the equation of motion is inadequate. For example, in the CAK model, stars of different $T_{\rm eff}$ and gravity have different $\dot{M}$ and V_∞, but the same velocity law. Paper I showed from first principles that early-type stars must deviate from the CAK velocity law, but the degree of departure could not be estimated. Corroborating evidence comes from observations at both UV (Abbott, Bohlin, and Savage 1982) and radio (Abbott, Bieging, and Churchwell 1981) wavelengths, which show that the density structure of the wind changes as stars evolve from the main sequence to supergiants. Because of this added uncertainty, the following comparison provides a much better—but still not decisive—test of the line-driven wind theory.

a) Terminal Velocity

In the theory of CAK, the terminal velocity is independent of the magnitude of the line acceleration; rather, it depends only on the parameter α, which measures the relative contribution of the optically thin and thick lines. As discussed by Abbott (1978*b*), if the value of α is independent of temperature and density, then all stars should obey the homology relation $V_\infty = \alpha/(1 - \alpha)^{1/2} V_{\rm esc}$, where $V_{\rm esc} \equiv [2GM(1 - \Gamma)/R_*]^{1/2}$. Table 2 shows that α is indeed nearly constant over the range $8000 \leq T_{\rm eff} \leq 50{,}000$ K, so that one would expect the winds of all OBA stars to obey $V_\infty \cong 1.0$–$1.5 V_{\rm esc}$.

Figure 8 plots the observed terminal velocities against the inferred escape velocities using the Copernicus data of Abbott (1978*b*), and the more recent *IUE* data of Cassinelli and Abbott (1981) and Garmany *et al.* (1981). (To be consistent with other work, $V_{\rm esc}$ was calculated using the cooler of the two effective temperature scales listed by Garmany *et al.*) Figure 8 shows the strong correlation between V_∞ and $V_{\rm esc}$, in agreement with theory. Both V_∞ and $V_{\rm esc}$ are uncertain by roughly $\pm 10\%$, which accounts for most of the scatter in Figure 8. It is obvious from Figure 8, however, that the constant of proportionality between V_∞ and $V_{\rm esc}$ is much larger than unity, in direct contradiction with theory.

Further, the discrepancy is systematic with $T_{\rm eff}$, as shown in Figure 9. Two important features of Figure 9 are: (1) There is a gradual increase in $V_\infty/V_{\rm esc}$ going

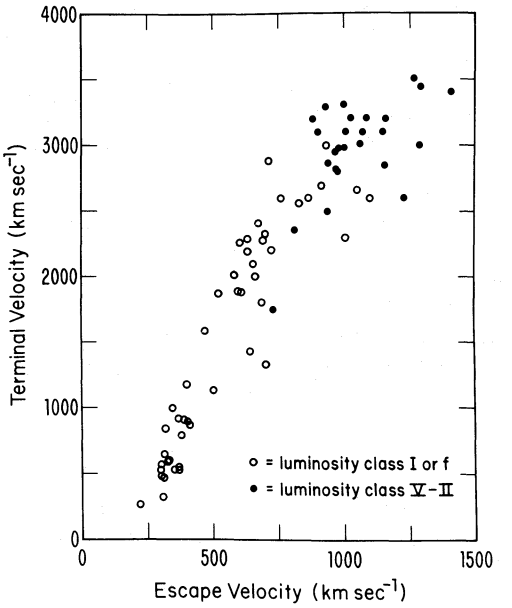

FIG. 8.—A summary of the terminal velocities observed from UV line profiles versus the photospheric escape velocity. The strong correlation is in agreement with the wind model of CAK.

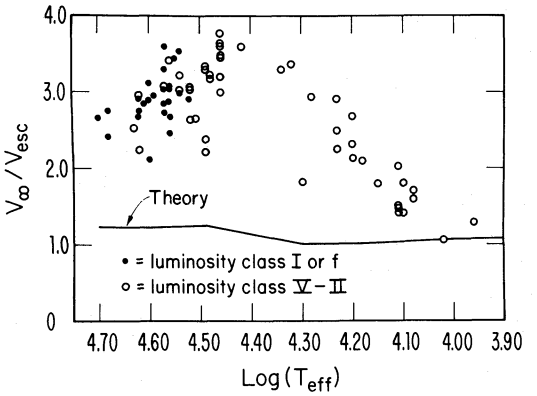

FIG. 9.—The dependence of the ratio V_∞/V_{esc} on effective temperature. The maximum of this ratio corresponds to spectral type O9–B0, with a sharp decrease in the ratio toward cooler stars, and a mild decrease in the ratio toward the hottest stars. The solid line is the constant of proportionality predicted by the CAK theory and the calculated line acceleration. The theory is a factor of ~2 too small for the O and early B stars.

from the early to the late O stars, with a maximum V_∞/V_{esc} at type O9.5, followed by a sharp decline in the ratio in the B stars. (2) It is the O and early B stars whose terminal velocities cannot be explained by the CAK wind model.

This discrepancy has also been noted by Panagia and Macchetto (1982), who proposed that the missing momentum needed to drive the large terminal velocities in O stars is provided by multiscattering of photons by strong resonance lines in the Lyman continuum. In their model the A and B supergiants do not multiscatter photons effectively because the lines are not as strong or as numerous.

To properly test their model requires calculating the effects of multiscattering using a realistic list of absorbing lines. In anticipation of this calculation, we note two potential problems for their explanation, which are evident from the data of Figure 9: (1) It is difficult to understand why the 30,000 K star is nearly twice as efficient at multiscattering as the 50,000 K star, i.e., why V_∞/V_{esc} declines in the hottest O stars. (2) The density of lines in B stars is greater than in O stars, as shown by Figure 7, which contradicts the basic assumption of the model. As shown in Figure 5*a*, however, the winds of B stars are dominated by iron group lines, while those of O stars are dominated by lighter ions. It may be that the resonance lines of Fe are not sufficiently opaque for multiscattering to operate effectively.

b) Mass Loss Rates

i) *Predicted Rates from the CAK Model*

The relationship of the mass loss rate to the line acceleration is best illustrated by integrating the momentum equation over mass. From Paper I, conservation of momentum is given by

$$V\frac{dV}{dr}+\frac{GM(1-\Gamma)}{r^2}-\frac{1}{\rho}\frac{dP}{dr}=a_L\,. \tag{15}$$

Applying

$$\int_{R_*}^{\infty} dr 4\pi r^2 \rho$$

to equation (15) and simplifying gives equation (86) of Paper I, or

$$\dot{M}V_\infty+\frac{1-\Gamma}{\Gamma}\tau_w\left(\frac{L}{c}\right)=B\left(\frac{L}{c}\right), \tag{16}$$

where $\dot{M}V_\infty$ is the rate momentum is being carried off by the wind; $[(1-\Gamma)/\Gamma]\tau_w L/c$ is the work done against gravity, where τ_w is the continuum optical depth of the wind; and BL/c is the rate at which momentum is transferred from the radiation to the gas, expressed in terms of the blocking factor

$$B\equiv\int_0^\infty \frac{dV}{V_{th}}\,t\mathcal{M}(t)\,, \tag{17}$$

which was discussed in a different context by equation (14).

Using the CAK velocity law, the gravity term becomes $[(1-\Gamma)/\Gamma]\tau_w L/c=[(1-\alpha)/\alpha]\dot{M}V_\infty$ and the blocking factor is $B=V_\infty/V_{th}\,k t_c^{1-\alpha}$, where t_c is the value of t at the critical point of the wind. Therefore, in the CAK model equation (16) is

$$\frac{1}{\alpha}\dot{M}V_\infty=\frac{V_\infty}{V_{th}}k t_c^{1-\alpha}\left(\frac{L}{c}\right). \tag{18}$$

Substituting the identity

$$t_c=\dot{M}V_{th}\Gamma(1-\alpha)/[L/c(1-\Gamma)\alpha]$$

into equation (18) and solving for $\dot{M}$ gives the CAK result:

$$\dot{M}=\frac{\alpha}{V_{th}}k^{1/\alpha}\left[\frac{(1-\alpha)\Gamma}{1-\Gamma}\right]^{1-\alpha/\alpha}\left(\frac{L}{c}\right). \tag{19}$$

ii) *Relationship of Mass Loss Rate to Gravity*

Common sense says that it takes more force to lift the same amount of matter out of a deeper gravitational well. This leads to the expectation that $\dot{M}$ should decrease with increasing gravity. Just the opposite is shown by equation (19), where $\dot{M}$ is independent of radius and depends on mass only through the constant $\Gamma\equiv\sigma_e L/4\pi GMc$.

To understand this apparent paradox, consider the simple example of a mass Δm which is given a velocity V_0 at a stellar surface by an impulse $I_0=V_0\Delta m$. The maximum mass is ejected when V_0 is a minimum, i.e., $V_0=V_{esc}$, and

$$\Delta m=I_0/V_{esc}\propto(R_*/M)^{1/2}\,. \tag{20}$$

This result is the basis for the intuitive feeling that $\dot{M}$ of a star should decrease with increasing gravity. Note, however, that if the impulse I_0 is not constant, but is proportional to V_{esc}, then the amount of mass which can be ejected is independent of gravity. This is essentially what prevails in radiatively driven winds.

If the blocking factor B were to be constant from star to star, equations (16) and (18) show that $\dot{M} \propto 1/V_\infty \propto 1/V_{esc} \propto (R_*/M)^{1/2}$, which is the expected result from equation (20) for a constant force impulse. In line-driven winds, however, the blocking factor is not constant, but varies according to $B \propto V_\infty$, as shown by equation (18). Thus, an increase in gravity is compensated by an increase in the radiative acceleration, as each line sweeps out a proportionately greater frequency interval of the emitted flux. The net result is a mass loss rate that is nearly independent of gravity. (This same conclusion also follows from the fact that the radiative flux and gravity both scale as r^{-2}, so their ratio is radius independent.)

iii) *Comparison of Calculated and Observed Rates for OBA Stars*

To predict the dependence of $\dot{M}$ on the stellar quantities L, M, and R_*, we substitute the mean relation for the calculated force multiplier, equation (12), into the CAK formula for the mass loss rate, equation (19). Using the equation of continuity, $\dot{M} = 4\pi\mu m_H N_e V r^2$, the value of the electron density N_e/W at $r = 1.5\ R_*$ and $V = V_{esc}$ can be expressed as $N_{11} = 3.8 \times 10^{15}\ \dot{M}/[M(1-\Gamma)R_*^3]^{1/2}$ cm^{-3}, or the force multiplier equals

$$\mathcal{M}(t) = k' t^{-\alpha} = 7.1 \left[\frac{\dot{M}}{(M(1-\Gamma)R_*^3)^{1/2}}\right]^{0.09} \left(\frac{Z}{Z_\odot}\right)^{1-\alpha} t^{-\alpha} . \quad (21)$$

Substituting the value of k' from equation (21) and $\bar{\alpha} = 0.56$ into the CAK formula and using the identity, $R_*^2 = L/(4\pi\sigma T_{eff}^4)$, gives a theoretical mass loss rate of

$$\dot{M}_{theory} = 1.4 \times 10^{-15} \times \frac{(L/L_\odot)^{1.98}(Z/Z_\odot)^{0.94}}{(M_{eff}/M_\odot)^{1.03}(T_{eff}/10^4\ \mathrm{K})^{0.02}} M_\odot\ \mathrm{yr}^{-1} , \quad (22)$$

where $M_{eff} \equiv M(1-\Gamma)$, and equation (22) is only valid for $50{,}000 \geq T_{eff} \geq 10{,}000$ K. To understand the scaling of equation (22), recall that stars of the same luminosity but cooler temperatures have smaller wind densities, which decreases the line acceleration. Stars at cooler temperatures, however, have more lines to absorb the radiation flux, which increases the line acceleration. These two factors effectively cancel in equation (22), giving a theoretical mass loss rate that has a negligible dependence on T_{eff}, or equivalently, on R_*.

The best empirical estimates of $\dot{M}$ come from the combination of radio and ultraviolet observations summarized in Figure 10. The radio data is from VLA detections of 16 OB stars at 5 GHz, taken from Abbott *et al.* (1980, 1981, and unpublished), and in principle these are the most reliable estimates possible of $\dot{M}$. Unfortunately, even with the high sensitivity of the VLA, only stars with $\dot{M} \gtrsim 10^{-6}\ M_\odot\ \mathrm{yr}^{-1}$ are detectable at radio frequencies. As shown by the analysis of Garmany *et al.* (1981), an accurate determination of $\dot{M}$ can also be made from UV data, if a star has at least two resonance lines which have detectable, but not saturated, violet-shifted absorption features. This is possible typically only if $\dot{M} \lesssim 10^{-6}\ M_\odot\ \mathrm{yr}^{-1}$, which makes the UV and radio data perfectly complementary. The 12 stars from the sample of Garmany *et al.* (1981) which have detectable, but not saturated, N V and C IV resonance lines are also plotted in Figure 10. The combined UV and radio data are fitted by the empirical relation

$$\dot{M}_{empirical} = 1.3 \times 10^{-16}(L/L_\odot)^{1.77}\ M_\odot\ \mathrm{yr}^{-1} . \quad (23)$$

Neither study finds a dependence of $\dot{M}$ on M or R_* that exceeds the $\sim$0.3 dex intrinsic scatter in the data.

In order to compare the observations of Figure 10 to the theoretical predictions of equation (22), one must choose a value for the stellar mass. To this end, $\dot{M}_{theory}$ was calculated using the sequence of (L, M_{eff}) values predicted by evolutionary models of stars with initial masses in the range of 20–100 $M_\odot$. The evolution calculations are from Chiosi (1981, private communication), using the empirical $\dot{M}$ versus L relation of the radio data of Abbott, Bieging, and Churchwell (1981*a*), and accounting for the effects of convective overshooting as described by Bressan, Bertelli, and Chiosi (1981). As the stars evolve from the main sequence to the point of hydrogen exhaustion, they trace out the range of predicted mass loss rates shown by the shaded area marked $\dot{M}_{CAK}$ in Figure 10.

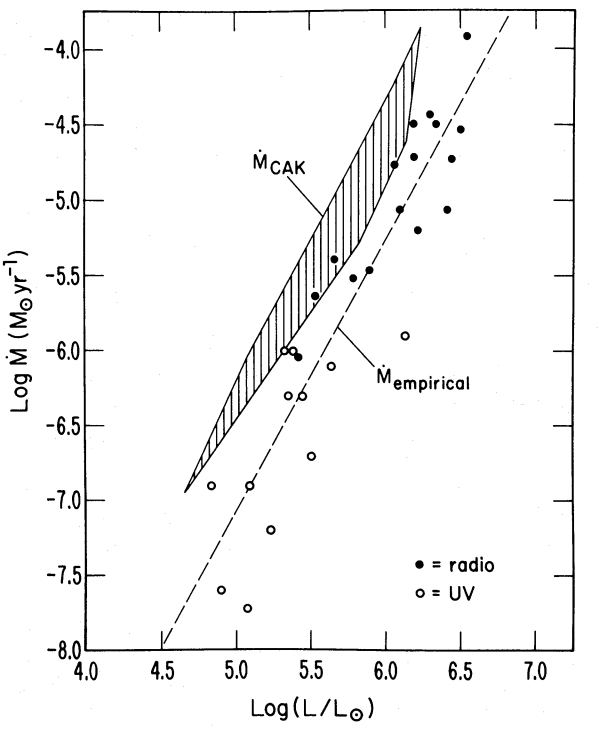

FIG. 10.—A comparison of observed and predicted mass loss rates for OB stars. The "radio" mass loss rates are from VLA data at 5 GHz. The "UV" mass loss rates are from high-resolution *IUE* observations of the N V and C IV resonance doublets. The shaded area gives the range of mass loss rates predicted by the CAK theory and the calculated line acceleration. The spread in predicted mass loss rates results from the range of possible masses which can be associated with stars of a given luminosity.

The comparison of observation and theory shown in Figure 10 establishes three main results:

1. *There are sufficient lines to drive the observed mass loss.* In fact, the predicted mass loss rates are systematically larger than the observed rates by a factor of 2. Since the uncertainty in the calculated radiation pressure is a factor of 2–3, the discrepancy shown in Figure 10 is not unexpected. The most likely explanation for the discrepancy is the ionization balance, since empirical ionization fractions give a line acceleration that is about a factor of 2 smaller than that calculated here.

2. *The predicted scaling of $\dot{M}$ with L agrees with observation.* For stars on or near the main sequence—where mass loss has not yet affected the stellar evolution—luminosity scales with initial mass as $L \propto M^2$, so equation (22) becomes $\dot{M}_{\rm theory} \propto L^{1.5}$. At the point of hydrogen exhaustion, all stars initially more massive than $\sim 60\ M_\odot$ have about the same final mass, so equation (22) becomes $\dot{M}_{\rm theory} \propto L^2$. The average dependence of $\dot{M}_{\rm theory}$ on L between these extremes agrees completely with the least squares fit to the observed data, which is indicated by the dashed line in Figure 10.

3. *The predicted dependence of $\dot{M}$ on $M_{\rm eff}$ is not yet observable.* As shown in Figure 10, the intrinsic scatter in the observed values of $\dot{M}$ and L is greater than the predicted range in $\dot{M}_{\rm theory}$ because of the $M_{\rm eff}$ term. The problem is especially acute for the stars of the highest luminosity for which the estimated values of L and M have the greatest uncertainty.

The primary culprit is the effective temperature scale, which is not well calibrated at the upper end of the O star sequence. The critical question is whether or not the same $T_{\rm eff}$ calibration applies to both evolved and main sequence stars. A change in the $T_{\rm eff}$ relationship between these two types of stars can potentially cause a bigger shift in the L/M ratio than that caused by the decrease in M during stellar evolution. For example, the prototype star ζ Puppis has an effective temperature which ranges from $50{,}000 \geq T_{\rm eff} \geq 33{,}000$ K, depending on the method employed. The corresponding range in the calculated bolometric correction is 1.3 mag (Morton 1969). Evolutionary tracks with mass loss suggest that ζ Pup has lost roughly one-fourth of its mass during its lifetime because of mass loss, which corresponds to a one-third decrease in $M_{\rm eff}$. Thus, the uncertainty in L because of the bolometric correction is greater than the increase in $\dot{M}_{\rm theory}$ resulting from the decreasing mass of the star.

A second difficulty for determining the empirical dependence on $M_{\rm eff}$ is that the masses, and hence the Γ factors, of very luminous stars are also quite uncertain. Masses drived from binary orbits are not well determined for supergiants because the strong, and often interacting, stellar winds affect the observed profiles and the interpretation of the derived velocity curve. Masses derived from evolutionary calculations suffer from uncertainty in the adopted values of $\dot{M}$, the metallicity, and the method of calculation (e.g., the treatment of convective overshooting).

A final complicating factor is that the observed mass loss rates come from stars which occupy a range of ~ 3 kpc in galactic radius. If the composition of these stars obeys the canonical relation $\Delta Z = -0.05$ dex kpc^{-1} (Peimbert 1979), then a dispersion of 0.15 dex in the observed $\dot{M}$ versus L is predicted by equation (22). This effect is smaller than the other uncertainties, but it may become significant when observations of very distant stars are considered, as discussed below in § IV*c*.

iv) *Comparison of Observed and Calculated Rates for F and G Supergiants*

For F and G supergiants, both the predicted and observed values of $\dot{M}$ are highly uncertain. Lambert, Hinkle, and Hall (1981) estimate mass loss rates of $\sim 7 \times 10^{-4}\ M_\odot$ yr^{-1} for ρ Cas (F8 Ia) and $\sim 8 \times 10^{-5}\ M_\odot$ yr^{-1} for HR 8752 (G0 Ia) from the inferred column densities of circumstellar CO. For both stars, the observations suggest that the mass loss is episodic, so eruptions may be a better term than winds to describe the outflow. The parameters of these two stars are similar to those of the $T_{\rm eff} = 6000$ K model in Table 3. Plugging the calculated line acceleration of Table 2 into equation (20) gives $\dot{M}_{\rm theory} = 2 \times 10^{-8}\ M_\odot$ yr^{-1} and $V_\infty = 110$ km s^{-1}.

This is four decades smaller than the derived rates of Lambert, Hinkle, and Hall (1981). However, there are two problems with the theory which affect the predicted rates: (1) No molecular lines are included in the calculated line acceleration, but it is obvious observationally that molecules are absorbing a large amount of radiation. (2) Likewise, the standard ionization balance using the fluxes and densities of Table 3 is much too high for the kinetic temperatures of ~ 2000 K derived by Lambert *et al.* for the circumstellar shells of ρ Cas and HR 8752. Decreasing the ionization temperature enhances the radiation pressure on the atomic lines. For example, the higher density model of Table 2 with $T_{\rm eff} = 6000$ K predicts $\dot{M} = 2 \times 10^{-6}\ M_\odot$ yr^{-1}, an increase of two decades over the standard ionization model.

Despite the large uncertainties, the above calculations strongly suggest that radiation pressure acts in concert with another mechanism to produce the observed mass loss. This is also consistent with the calculations of Abbott (1979), who showed that radiation pressure can sustain, but not self-initiate, winds in F and G supergiants.

c) *Dependence on Metallicity*

The predicted dependence of $\dot{M}$ on Z has both direct and indirect observational consequences. The direct consequence is a sharp reduction in the mass loss rates for OB stars of small metallicity, such as those in the Magellanic Clouds. Unfortunately, such a decrease is difficult to detect, because these stars are too faint for radio or 10 μm infrared observations, and high-resolution UV observations are possible only for the most luminous stars, for which the resonance lines are saturated.

The dependence of $\dot{M}$ on Z is indirectly observable

through differences in the H-R diagram between galactic and extragalactic regions of different metallicity. As noted by several studies (e.g., Chiosi, Nasi, and Sreenivasan 1978; Maeder 1980), small changes in $\dot{M}$ during the hydrogen-burning phase of an OB star cause dramatic changes in the subsequent evolution of the star.

Observational evidence for this effect is given by Maeder, Lequeux, and Azzopardi (1980), who find that the observed ratio of the number of red supergiants to Wolf-Rayet stars, N_R/N_{WR}, becomes very large in regions of lower metallicity in our Galaxy and in the Magellanic Clouds. (Note, however, that these statistics are contested by Bertelli and Chiosi 1982.) In the scenario of Maeder *et al.*, a bigger rate of mass loss during the hydrogen burning phase results in a smaller fractional mass for the hydrogen envelope during helium burning in the red supergiant phase, which in turn reduces the time spent before a red supergiant sheds its envelope and becomes a Wolf-Rayet star. More mass loss during hydrogen burning therefore results in a smaller N_R/N_{WR} ratio.

Maeder *et al.* find that N_R/N_{WR} increases from 0.14 to 13.0 as Z decreases from roughly 0.03 to 0.01. The predicted dependence of $\dot{M} \propto Z$ for OB stars therefore goes in the right direction to explain the increase in N_R/N_{WR}. However, the entire factor of 100 change in N_R/N_{WR} cannot be caused by only a factor of 3 increase in $\dot{M}$ in the blue supergiant phase. Other factors, such as $\dot{M}$ in the red supergiant phase, must also be sensitive to Z in order to explain the observed gradient.

d) Wolf-Rayet Stars

The mass loss rates observed from Wolf-Rayet stars also pose a test of the dependence of $\dot{M}$ on chemical composition. Radio observations by Abbott, Bieging, and Churchwell (1982), as well as Hogg (1982), show that Wolf-Rayet stars as a class have rates of mass loss in the range $4 \times 10^{-5}\ M_\odot\ \mathrm{yr}^{-1} \geq \dot{M} \geq 1 \times 10^{-5}\ M_\odot\ \mathrm{yr}^{-1}$. These mass loss rates are an order of magnitude larger than those of O stars of comparable luminosity, although such a comparison is somewhat uncertain because the bolometric luminosities of the Wolf-Rayet stars are not reliably known.

The most obvious difference between OB stars and Wolf-Rayet stars is their chemical composition. A major motivation for the present work was to determine if the enrichment of Wolf-Rayet atmospheres by nuclear burning could explain the extraordinary rates of mass loss from these stars. The answer is no. As shown in Figure 3*a* and described in § III*b*, there is no increase in the line acceleration of the WN sequence, and at most a factor of 2 increase in the line acceleration of the WC sequence. Using equation (19), this means that the mass loss rate could be enhanced by up to a factor of 3 in a WC star which is nearing the end of the stage of core helium burning.

The standard CAK model of line driven winds does not seem capable of explaining the winds from W-R stars. This implies either that the standard model is inadequate for the conditions of W-R stars, or that some other physical process is contributing to the mass outflow. Abbott (1982) discusses several approximations of the CAK model which are adequate for OB stars, but fail completely for Wolf-Rayet stars. It is not known whether or not remedying these inadequacies will bring the line-driven wind model into agreement with observations for Wolf-Rayet stars.

V. SUMMARY AND CONCLUSIONS

The acceleration from spectral lines in an expanding atmosphere is presented for a broad range of temperatures, densities, chemical compositions, and values of the expansion parameter $\mathrm{t} = \sigma_e \rho V_{th}/(dV/dr)$. From the tabulated data, radiation wind models can be constructed for stars of spectral types O–G, and any luminosity or metallicity. The main improvement of this work over previous calculations is that accurate and complete atomic data were used to compute line opacity. Errors in the calculated acceleration because of omitted or inaccurate *gf*-values are typically less than a few percent.

Two sources of error remain in the calculated line acceleration: the ionization balance and the effect of overlapping lines on the radiative transfer in the wind. The ionization balance predicted by different model atmospheres was compared to empirical ionization fractions determined from UV observations. In all cases, the higher the state of ionization, the smaller the line acceleration. The anomalously high stages of ionization observed in OB star winds hinder, rather than help, the radiative acceleration. The overall uncertainty in the calculated line acceleration because of the ionization balance is less than a factor of 2.

A test case of the effects of line overlap showed that for $T_{\mathrm{eff}} = 40{,}000$ K more than one-half of the acceleration comes from lines which overlap in frequency with another line somewhere in the wind. Line-locking among multiplets is the rule, rather than the exception. Exact calculations by Castor (1979) and Olson (1981) show that the acceleration is usually enhanced at large radii by line overlap, because the photons multiscatter from one side of the envelope to the other. At small radii, line overlap reduces the size of the line acceleration. This work neglects line overlap. The calculated line acceleration therefore approximates the true acceleration at intermediate radii, but is likely an overestimate at small radii and an underestimate at large radii. The effects of line overlap are by far the largest source of uncertainty in these calculations.

The line acceleration is remarkably constant over the temperature range $50{,}000 \geq T_{\mathrm{eff}} \geq 10{,}000$ K. In this T_{eff} range, the numerical values of the line acceleration given in Table 2 are approximated to within a factor of 3 by the analytic expression

$$\mathcal{M}(\mathrm{t}) = 0.28\mathrm{t}^{-0.56}(N_{11})^{0.09}(Z/Z_\odot)^{0.44}\ , \qquad (24)$$

where N_{11} is the value of (N_e/W) in units of 10^{11} cm^{-3}, and $Z/Z_\odot$ is the mass fraction of metals relative to those tabulated for the Sun by Cameron (1973). Equation (24) shows that the line acceleration increases with increasing metallicity, because metals are the primary absorbers of

radiative momentum, and also with increasing density, because the lower stages of ionization have more lines.

The line acceleration arises from many individual lines from a broad range of elements, so the net radiation pressure is insensitive to the individual behavior of any particular line or ion. The number of lines required to accurately represent the acceleration ranges from several hundreds for small values of t ($t \lesssim 10^{-6}$), to several thousands for large values of t ($t \gtrsim 10^{-2}$). Roughly half the acceleration comes from optically thick lines; the remainder is provided by the cumulative contribution of the more numerous optically thin lines. Roughly 90% of the acceleration arises from lines whose lower states are either ground or metastable levels.

Stellar winds increase line blanketing, because the opaque lines are Doppler-shifted across a greater bandwidth. Figure 7 shows the sort of flux-blocking that can occur in high-density winds ($t = 10^{-3}$, or $\dot{M} \sim 10^{-5} M_\odot$ yr^{-1}). Such line blanketing causes major changes in the temperature structure and the emergent continuum flux (Hummer 1981). Line-blanketing effects become significant for mass loss rates exceeding $\sim 10^{-6} M_\odot$ yr^{-1}.

The CAK model predicts a relation between the terminal velocity and the photospheric escape velocity of $V_\infty = [\alpha/(1-\alpha)]^{1/2} V_{esc}$. The values of α calculated here predict a constant of proportionality ranging from 1.4 for the O stars to 1.0 for the B and A stars. Observationally, there is a very strong correlation between V_∞ and V_{esc}—which supports the theory—but the constant of proportionality is wrong, as shown in Figure 9. This discrepancy has been explained within the confines of line-driven wind theory by Panagia and Macchetto (1982), who showed that multiscattering of photons in the O stars provides the missing momentum needed to attain the large observed terminal velocities.

A major objective of these calculations was to determine if there are sufficient lines to drive the large rates of mass loss observed in hot stars. Applying the CAK wind model to the calculated line acceleration gives the predicted mass loss rates of equation (22). Figure 10 compares this prediction to radio and UV observations of OB stars. Over the four decades of observed mass loss rates, theory and observation agree to within a factor of 2. This is a remarkable agreement, considering that the theory was calculated from first principles, with no free or adjustable parameters. The remaining discrepancy between theory and observation most likely results from either the ionization balance or the treatment of overlapping lines. We conclude that radiation pressure on spectral lines is the dominant mechanism driving the mass loss from OB stars.

This is not the case for Wolf-Rayet stars. The inferred mass loss rates of W-R stars are typically a factor of 10 larger than those of O stars of comparable luminosity. These calculations show that the large difference in mass loss rates does not result from the differences in chemical composition between the O and W-R stars. There is no predicted enhancement in $\dot{M}$ for the WN sequence because of abundance effects, and at most a factor of 3 enhancement in $\dot{M}$ for stars of the WC sequence. This means that either (1) the derived values of $\dot{M}$ and M_{bol} are systematically in error for the W-R stars, (2) the mass loss is driven by radiation pressure but the CAK wind model is not applicable to W-R stars (cf. Abbott 1982), or (3) another mechanism is responsible for the winds of W-R stars.

The fraction of the radiative momentum that is absorbed by atomic lines drops off sharply for stars cooler than $T_{eff} = 10{,}000$ K. The predicted mass loss rates for F and G supergiants are correspondingly smaller than those of OBA supergiants by factors of roughly 10 and 100, respectively. Comparison to the high envelope densities derived for the F and G supergiants ρ Cas and HR 8752 suggests the radiation pressure abets, rather than dominates, the mass loss from these stars.

Line-driven wind theory predicts a nearly linear dependence of $\dot{M}$ on Z. The consequences of mass loss on the observed spectrum, on the interstellar medium, and on the subsequent evolution of the star will also vary with metallicity. These differences should be observable in stellar systems in other galaxies or in distant regions of our Galaxy. As one such example, the ratio of red supergiants to Wolf-Rayet stars is linked to metallicity via the mass loss rate during the blue supergiant phase, as discussed by Maeder, Lequeux, and Azzopardi (1980). Observations providing a more direct test of the dependence of $\dot{M}$ on Z in OB stars would be very worthwhile.

This work benefited from discussions with John Castor, and the support of National Science Foundation grants AST 79-18388 and AST 80-19874 to the University of Colorado.

REFERENCES

Abbott, D. C. 1977, Ph.D. thesis, University of Colorado.
———. 1978*a*, *J. Phys. B*, **11**, 3479.
———. 1978*b*, *Ap. J.*, **225**, 893.
———. 1979, in *IAU Symposium 83, Mass Loss and Evolution of O-type Stars*, ed. P. S. Conti and C. deLoore (Dordrecht: Reidel), p. 237.
———. 1980, *Ap. J.*, **242**, 1183.
———. 1982, in *IAU Symposium 99, Wolf-Rayet Stars: Observations, Physics, and Evolution*, ed. C. deLoore and A. Willis (Dordrecht: Reidel), in press.
Abbott, D. C., Bieging, J. H., and Churchwell, E. 1981, *Ap. J.*, **250**, 645.
———. 1982, in *IAU Symposium 99, Wolf-Rayet Stars: Observations, Physics and Evolution*, ed. C. deLoore and A. Willis (Dordrecht: Reidel), in press.
Abbott, D. C., Bieging, J. H., Churchwell, E., and Cassinelli, J. P. 1980, *Ap. J.*, **238**, 196.
Abbott, D. C., Bohlin, R. C., and Savage, B. D. 1982, *Ap. J. Suppl.*, in press.
Anderson, T., Biemont, E., and Peterson, P. 1977, *J. Quant. Spectrosc. Rad. Transf.*, **17**, 389.
Anderson, T., Desesquelles, J., Jessen, K. A., Sorensen, G. 1970, *J. Opt. Soc. Am.*, **60**, 1199.
Aymar, M. 1973, *Nucl. Instr. Meth.*, **110**, 211.
Barlow, M. J., and Cohen, M. 1977, *Ap. J.*, **213**, 737.

Barrette, L., Knystantas, E. J., Neveu, B., and Drounin, R. 1970, *Nucl. Instr. Meth.*, **90**, 59.
Bashkin, S., and Martinson, I. 1971, *J. Opt. Soc. Am.*, **61**, 1686.
Baudinet-Robinet, Y., Dumont, P. D., and Garnir, H. P. 1979, *J. Phys. Colloq.*, **40**, C1-175.
Berry, H. G., Bickel, W. S., Bashkin, S., Desesquelles, J., and Schectman, R. M. 1971, *J. Opt. Soc. Am.*, **61**, 947.
Bertelli, G., and Chiosi, C. 1982, in *IAU Symposium 99, Wolf-Rayet Stars: Observations, Physics and Evolution*, ed. C. deLoore and A. Willis (Dordrecht: Reidel), in press.
Bressan, A. G., Bertelli, G., and Chiosi, C. 1981, preprint.
Buchet, J. P., Buchet-Poulizac, M. C., and Druetta, M. 1978, *Phys. Scr.*, **18**, 496.
Buchet, J. P., Poulizac, M. C., and Carre, M. 1972, *J. Opt. Soc. Am.*, **62**, 623.
Cameron, A. G. W. 1973, in *Explosive Nucleosynthesis*, ed. D. Schramm and W. D. Arnett (Austin: University of Texas Press), p. 3.
Cassinelli, J. P. 1979, *Ann. Rev. Astr. Ap.*, **17**, 275.
Cassinelli, J. P., and Abbott, D. C. 1981, in *The Universe at Ultraviolet Wavelengths*, ed. R. D. Chapman (NASA CP-2171), p. 127.
Cassinelli, J. P., Waldron, W., Sanders, W. T., Harnden, F. R., Rosner, R., and Vaiana, G. S. 1981, *Ap. J.*, **250**, 677.
Castor, J. I. 1974*a*, *M.N.R.A.S.*, **169**, 279.
———. 1974*b*, unpublished (calculations are described in CAK).
———. 1979, in *IAU Symposium 83, Mass Loss and Evolution of O-type Stars*, ed. P. S. Conti and C. deLoore (Dordrecht: Reidel), p. 175.
Castor, J. I., Abbott, D. C., and Klein, R. I. 1975, *Ap. J.*, **195**, 157 (CAK).
———. 1976, in *Physiques des Mouvements dans les Atmospheres Stellaires*, ed. R. Cayrel and M. Steinberg (Paris: Cent. Nat. Rech. Sci.).
Ceyzeriat, P., Denis, A., Desesquelles, J., Druetta, M., and Poulizac, M. C. 1970, *Nucl. Instr. Meth.*, **90**, 103.
Chiosi, C., Nasi, E., and Sreenivasan, S. R. 1978, *Astr. Ap.*, **73**, 103.
Conti, P. S. 1978, *Ann. Rev. Astr. Ap.*, **16**, 371.
———. 1982, in *IAU Symposium 99, Wolf-Rayet Stars: Observations, Physics and Evolution*, ed. C. deLoore and A. Willis (Dordrecht: Reidel), in press.
Curtis, L. J., Martinson, I., and Buchta, R. 1971, *Phys. Scr.*, **3**, 197.
Denis, A. 1969, *Comp. Rend.*, **268B**, 1176.
Druetta, M. 1969, *Comp. Rend.*, **269B**, 1154.
Druetta, M., Poulizac, M. C., and Ceyzeriat, P. 1971, *J. Phys. B*, **4**, 1070.
Druetta, M., Poulizac, M. C., and Desesquelles, J. 1970, *J. Opt. Soc. Am.*, **60**, 1463.
Dufay, M., Denis, A., and Desesquelles, J. 1970, *Nucl. Instr. Meth.*, **90**, 85.
Dufay, M., Gaillard, M., and Carre, M. 1971, *Phys. Rev. A*, **3**, 1367.
Dumont, P. D. 1972, *Physica*, **62**, 104.
Dumont, P. D., Baudinet-Robinet, Y., Garnir, H. P., Biemont, E., and Grevesse, N. 1979, *Phys. Rev. A*, **20**, 1347.
Garmany, C. D., Olson, G. L., Conti, P. S., and Van Steenberg, M. 1981, *Ap. J.*, **250**, 660.
Heroux, L. 1967, *Phys. Rev.*, **153**, 156.
Hesser, J. E. 1968, *Phys. Rev.*, **174**, 68.
Hogg, D. 1982, in *IAU Symposium 99, Wolf-Rayet Stars: Observations, Physics and Evolution*, ed. C. deLoore and A. Willis (Dordrecht: Reidel), in press.
Hummer, D. G. 1981, preprint.
Hummer, D. G., and Norcross, D. W. 1974, *M.N.R.A.S.*, **168**, 263.
Irwin, D. J. G., and Livingston, A. E. 1973, *Can. J. Phys.*, **51**, 848.
Irwin, D. J. G., Livingston, A. E., and Kernahan, J. A. 1973*a*, *Nucl. Instr. Meth.*, **110**, 105.
———. 1973*b*, *Nucl. Instr. Meth.*, **110**, 111.
Kernahan, J. A., Denis, A., and Drounin, R. 1971, *Phys. Scr.*, **4**, 49.
Kernahan, J. A., Pinnington, E. H., Donnelly, K. E., O'Neill, J. A., and Brooks, R. L. 1979, *J. Phys. Colloq.*, **40**, C1-180.
Klein, R. I., and Castor, J. I. 1978, *Ap. J.*, **220**, 902.
Knystantas, E., Barrette, L., Neveu, B., and Drounin, R. 1971, *J. Quant. Spectrosc. Rad. Transf.*, **11**, 75.
Kurucz, R. L. 1979, *Ap. J. Suppl.*, **40**, 1.
———. 1981, SAO Special Report No. 390.
Kurucz, R. L., and Peytremann, E. 1975, SAO Special Report No. 362.
Lamb, S. A., Iben, I., and Howard, W. M. 1976, *Ap. J.*, **207**, 209.
Lambert, D. L., Hinkle, K. H., and Hall, D. N. B. 1981, *Ap. J.*, **248**, 638.
Lamers, H. J. G. L. M., and Morton, D. C. 1976, *Ap. J. Suppl.*, **32**, 715.
Liljeby, L., Lindgard, A., Maunervik, S., Veje, E., and Jelenkovic, B. 1980, *Phys. Scr.*, **21**, 805.
Lin, C. C., Irwin, J. G., Kernahan, J. A., Livingston, A. E., and Pinnington, E. H. 1972, *Can. J. Phys.*, **50**, 2496.
Livingston, A. E., Irwin, D. J. G., and Pinnington, E. H. 1972, *J. Opt. Soc. Am.*, **62**, 1303.
Lucy, L. B. 1982, *Ap. J.*, **255**, 286.
Lucy, L. B., and Solomon, P. 1970, *Ap. J.*, **159**, 879.
Maeder, A. 1980, *Astr. Ap.*, **92**, 101.
Maeder, A., Lequeux, J., and Azzopardi, M. 1980, *Astr. Ap.*, **90**, L17.
Martinson, I., Berry, H. G., Bickel, W. S., and Oona, H. 1971, *J. Opt. Soc. Am.*, **61**, 519.
McIntyre, L. C., Donahue, D. J., and Bernstein, E. M. 1978, *Phys. Scr.*, **17**, 5.
Mihalas, D. 1972, *Non-LTE Model Atmospheres of B and O Stars*, NCAR TN/STR-76.
———. 1978, *Stellar Atmospheres*, 2nd Edition (San Francisco: Freeman).
Morton, D. C. 1969, *Ap. J.*, **158**, 629.
———. 1978, *Ap. J.*, **222**, 863.
Nicolaides, C. A., Beck, D. R., and Sinanoglu, O. 1973, *J. Phys. B*, **6**, 62.
Nussbaumer, H. 1969*a*, *M.N.R.A.S.*, **145**, 141.
———. 1969*b*, *Astro. Letters*, **4**, 183.
———. 1971, *Ap. J.*, **170**, 93.
Nussbaumer, H., and Storey, P. J. 1979, *Astr. Ap.*, **74**, 244.
Olson, G. L. 1982, *Ap. J.*, **255**, 267.
Olson, G. L., and Castor, J. I. 1981, *Ap. J.*, **244**, 179.
Panagia, N., and Macchetto, F. 1982, *Astr. Ap.*, in press.
Peimbert, M. 1979, in *The Large-Scale Characteristics of the Galaxy*, ed. W. B. Burton (Dordrecht: Reidel), p. 79.
Pinnington, E. H. 1970, *Nucl. Instr. Meth.*, **90**, 93.
Saraph, H. 1980, *J. Phys. B*, **13**, 3129.
Sinanoglu, O. 1973, *Nucl. Instr. Meth.*, **110**, 193.
Smith, W. H. 1978, *Phys. Scr.*, **17**, 513.
Vanbeveren, D., and Doom, C. 1980, *Astr. Ap.*, **87**, 77.
Victor, G., Stewart, R., and Laughlin, C. 1976, *Ap. J. Suppl.*, **31**, 237.
Westhaus, P., and Sinanoglu, O. 1969, *Phys. Rev.*, **183**, 56.
Wiese, W. L., Smith, M. W., and Glennon, B. W. 1966, *Atomic Transition Probabilities* (NBS 4-1).

DAVID C. ABBOTT: Joint Institute for Laboratory Astrophysics, Mail Code 440, University of Colorado, Boulder, CO 80309